

Review

Petrochronology of Monazite-Bearing Garnet Micaschists as a Tool to Decipher the Metamorphic Evolution of the Alpine Basement

Bernhard Schulz 

Institute of Mineralogy, Economic Geology and Petrology, TU Bergakademie Freiberg, Brennhausgasse 14, D-09599 Freiberg, Saxony, Germany; bernhard.schulz@mineral.tu-freiberg.de

Abstract: Garnet-bearing metapelites in the Helvetic and Austroalpine pre-Mesozoic polymetamorphic basement are characterised by pressure-temperature path segments reconstructed by microstructurally controlled geothermobarometry, and the Th-U-Pb monazite age distribution pattern revealed by the electron probe microanalyser (EPMA). In the Helvetic Aiguilles Rouges Massif and the Austroalpine Oetztal-Stubai basement to the NW an Ordovician-to-Silurian high temperature event preceded a pressure-dominated Carboniferous metamorphism. In the Austroalpine basement units to the south of the Tauern Window, the maximal pressures of the Carboniferous amphibolite-facies metamorphism range from 12 to 6 kbar. The decompressional P-T path segments signal a transition to low pressure conditions. A subsequent high pressure overprint is restricted to the Prijakt Subgroup unit in the Schobergruppe and documented by Cretaceous monazite crystallisation at 88 ± 6 Ma. In the Austroalpine Saualpe basement to the SE, a distinct early Permian metamorphism which started at low pressures of ~ 4 kbar/500 °C and reached maximal 6 kbar/600–650 °C predated the intrusion of Permian pegmatites. Permian monazite crystallised in line with the intrusion of pegmatites. Corona microstructures around the Permian monazites indicate retrogression previous to a Cretaceous high pressure metamorphism. That way, pressure-temperature-time paths resolve the spatial and temporal evolution in the polymetamorphic Alpine basement prior to the Tertiary collision.



Citation: Schulz, B. Petrochronology of Monazite-Bearing Garnet Micaschists as a Tool to Decipher the Metamorphic Evolution of the Alpine Basement. *Minerals* **2021**, *11*, 981. <https://doi.org/10.3390/min11090981>

Academic Editors: Manuel Roda and Jean-Marc Lardeaux

Received: 26 July 2021

Accepted: 6 September 2021

Published: 9 September 2021

Publisher's Note: MDPI stays neutral with regard to jurisdictional claims in published maps and institutional affiliations.



Copyright: © 2021 by the author. Licensee MDPI, Basel, Switzerland. This article is an open access article distributed under the terms and conditions of the Creative Commons Attribution (CC BY) license (<https://creativecommons.org/licenses/by/4.0/>).

Keywords: polymetamorphism; geothermobarometry; Th-U-Pb monazite dating; garnet; Austroalpine; Helvetic; pre-Variscan; Carboniferous; Permian; Cretaceous

1. Introduction

A major part of the Alps is composed of basement units. These units can be assigned to the continental Northern European Plate, to the overriding Austroalpine parts of the Adriatic-Apulian Plate, and to metamorphosed Mesozoic ophiolites and sediments belonging to the Penninic Ocean in between [1]. Many of these units underwent polymetamorphism [2]. Both, the European and the Adriatic-Apulian Plate, bear the heritage and relics of pre-Mesozoic orogenies [3,4]. Pioneering petrological studies for the recognition of metamorphic pressure-temperature-time (P-T) paths [5], and also radiochronological work [6–8], have been performed in the Alpine basement. Ordovician-to-Silurian, Carboniferous and Permian events, followed by the Alpine Cretaceous and Tertiary metamorphism have been reported [2]. In this complex tectonic and metamorphic frame of the Alpine basement, the dating of individual metamorphic events is difficult. The Sm-Nd, Lu-Hf, U-Pb and Rb-Sr dating of metamorphic minerals turned out to be suitable methods. U-Pb zircon dating potentially fails to date metamorphism in the greenschist to amphibolite facies and also in many high grade metamorphic rocks due to high closure temperatures. The Ar-Ar, K-Ar and Rb-Sr isotope systems date the late cooling history and may be severely disturbed not only in polymetamorphic settings. The chemical Th-U-Pb dating of monazite by a texturally controlled in situ electron probe microanalysis (EPMA) provides an interesting alternative, especially in polymetamorphic terrains [9–11]. Monazite is a

common accessory phase in peraluminous granite and in Ca-poor and Al-rich metapsammopelites at all metamorphic grades above the upper greenschist facies [12]. The appearance of garnet-bearing assemblages in many of such metapsammopelites provides the opportunity for a partial quantification of the pressure-temperature (P-T) evolution by geothermobarometry and/or pseudosection modelling. In combination with the EPMA Th-U-Pb monazite dating, this opens a great potential for the reconstruction of P-T-time paths of metamorphism. This combined approach has been applied in exemplary case studies on garnet-bearing micaschists and gneisses in the Aiguilles Rouges External Massif of the Helvetic Domain (European Plate) and to several different basement parts belonging to the Austroalpine part of the Adriatic-Apulian Plate. It is possible to distinguish basement units by their pre-Tertiary P-T-time (P-T-t) paths of polymetamorphism.

2. Materials and Methods

2.1. Basement Units in the Alps

The basement in the Alps can be subdivided into the metamorphosed remnants of the Mesozoic sediments and ophiolites assigned to the former Penninic ocean, and the pre-Mesozoic basement areas which belong to the European and Adriatic-Apulian plates (Figure 1a). Many parts of the pre-Mesozoic basement were highly transformed during the Alpine metamorphic overprint. In the External Massifs of the European Plate and in the Austroalpine domain of the Adriatic-Apulian microplate, there are crustal segments with minor overprint; thus, giving the possibility to recognize older lithologies and structures. Prior to their Alpine overprint, the pre-Mesozoic basement areas underwent a complex magmatic and metamorphic evolution [3,4]. Sedimentation along the north-Gondwana margin started in the Neoproterozoic. A detrital input from East-Gondwanan cratonic sources is dominant in the Austroalpine basement units [13]. During the Neoproterozoic-Lower Cambrian period, contemporaneous to the Cadomian orogenic evolution, basement units of the European Plate and the Northwestern Austroalpine realm belonged to an active margin setting [4,13–17]. The subsequent Ordovician evolution of the Alpine basement has not sufficiently been resolved yet. Numerous and widespread intrusions of I- and S-type granitoids (480–450 Ma) may signal a prolongation of the Cambrian active margin setting during the Ordovician [16]. An Ordovician subduction-collision cycle with associated metamorphism and igneous intrusions was also discussed [18,19]. Partial anatexis probably resulted from a thermal event triggered by crustal extension at 450–430 Ma. Nevertheless, in the Austroalpine realm (Figure 1a), the Ordovician plutonism allows to discriminate pre-Early Ordovician basement units with various granitoids, now orthogneisses, from post-Early Ordovician phyllite and quartzphyllite units with the corresponding volcanic rocks and volcanosediments [4]. Since the late Ordovician in south-eastern parts of the Austroalpine realm, a passive margin setting and crustal extension lasted until the opening of the Paleotethys Ocean during the Devonian. Many Alpine basement areas were then involved in the Variscan orogenic events in the Carboniferous, including continental subduction and then continental collision of the peri-Gondwanan margin with Laurussia [4]. The resulting assemblage of Pangea, then, underwent Permian, Triassic and Jurassic extension periods. The early Meliata-Hallstatt ocean separated basement units within the Austroalpine domain. The later Penninic ocean opened between the Adriatic-Apulian Plate to the south and the European Plate to the north. Both oceans were successively subducted previous to successive continental collisions at Cretaceous and Tertiary times, leading to the build-up of the Alpine mountain chain [1]. As a consequence of this multistage geodynamic evolution, in the metamorphic maps of the Alps, basement units with pre-Variscan, Variscan (Carboniferous), Permian, Cretaceous (Eo-Alpine, Early Alpine) and Tertiary (Late Alpine) metamorphism were distinguished [2,20]. Furthermore, polymetamorphic basement units with a pre-Mesozoic metamorphism at higher grades which were overprinted by a single or both Alpine metamorphic events at lower grades, and units with Alpine higher grade metamorphism subsequent to the pre-Mesozoic events have been recognized. Radiometric ages between ~300 and ~200 Ma from metamor-

phic rocks of the Austroalpine basement have long been considered as “Variscan-Alpine mixed” ages [21]. However, in the light of the increasing amount of data in this age range, a distinct high temperature low pressure Permian metamorphic event has been postulated. Apparently, this event was associated with the intrusion of Permian pegmatites at 270–250 Ma [22–24]. These were arranged along a linear zone extending from the southern Oetztal basement with the Martell granite, passing the Basement to the south of the Tauern Window and appearing also in the Saualpe and Koralpe basement [25–27]. A large zone of crustal extension was inferred for this event [22]. At least in some of the Austroalpine units, where Permian pegmatites intruded already foliated host rocks, these allow an evaluation if Alpine deformation overprinted pre-Permian structures.

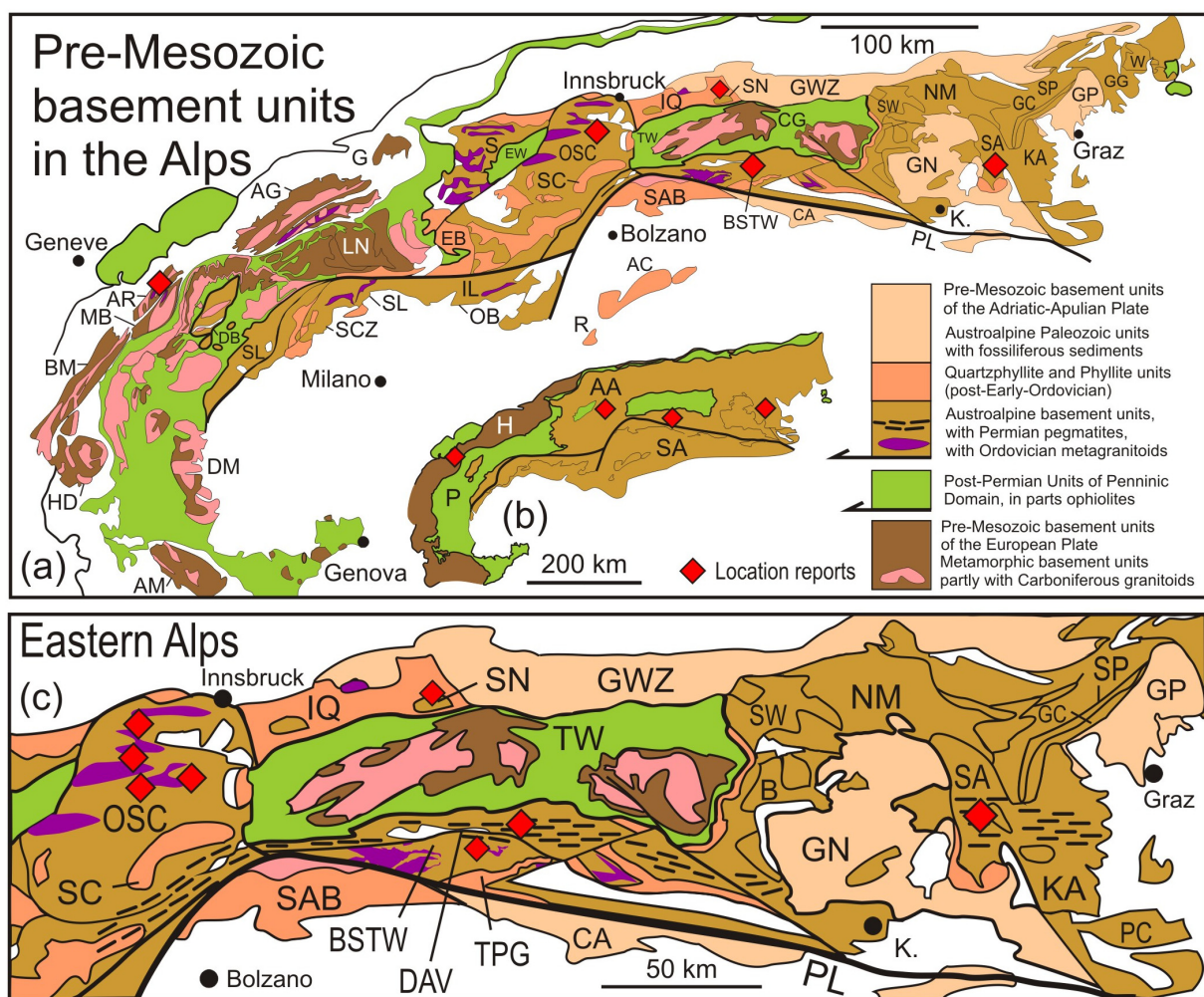


Figure 1. (a) Pre-Mesozoic basement units in the Alps [4]. (b) Subdivision of the basement units in Austroalpine (AA), Helvetic (H), Penninic (P) and South Alpine (SA) Domains. (c) Basement units in the Austroalpine Domain with locations of reports (red marks). Basement units and massifs, and major tectonic lines: AC Agordo-Cereda; AG Aar-Gotthard; AM Argentera Massif; AR Aiguilles Rouges Massif; B Bundschuh; BM Belledonne Massif; BSTW Basement South of Tauern Window; CA Carnic Alps; CG Central Gneisses; DAV Deferegggen-Antholz-Vals Line; DB Dent Blanche; DM Dora Maira; EB Err-Bernina; EW Engadine Window; G Glarus; GC Gleinalm Complex; GG Grogneis Complex; GN Gurktal nappes; GP Graz Paleozoic; GWZ Greywacke Zone; HD Haute Dauphiné; IL Insubric Line; IQ Innsbruck Quartzphyllite; KA Koralpe; LN Lepontine Nappes; MB Mont Blanc; NM Niedere Tauern and Micaschist Complexes; OB Orobic Basement; OSC Oetztal-Stubai Complex; PC Pohorje Complex; PL Periadriatic Lineament; R Recoaro; S Silvretta; SA Saualpe; SAB South Alpine Basement; SC Schneeberg Complex; SCZ Seconda Zona Diorite Kinzigite; SL Sesia-Lanzo Zone; SN Steinkogel nappe; SP Speik Complex with Kraubath ophiolite; TPG Thurntaler Phyllite Group; TW Tauern Window; W Wechsel Gneiss Complex.

The reconstruction of pressure-temperature-time (P-T-t) paths by the methods of petrochronology is important to decipher the evolution of each unit in the basement puzzle of the Alps. Case studies in four basement areas are reviewed (Figure 1a):

- (1) The Aiguilles Rouges Massif (AR) belongs to the Alpine External Massifs and is part of the European Plate. It underwent a high pressure Carboniferous (“Variscan”) metamorphism, and there were indications of an Ordovician-to-Silurian event. There is a low-grade Alpine overprint.
- (2) The Oetztal-Stubai Complex (OSC) is part of the western Austroalpine domain. There are indications of an Ordovician event with migmatism. A Carboniferous metamorphism with formation of eclogites is predominant. Towards the SE of the OSC, an increasing Cretaceous overprint reaching the amphibolite facies is obvious.
- (3) The basement to the south of the Tauern Window (BSTW) and the Steinkogel Nappe (SN) to the north of the Tauern Window underwent Carboniferous metamorphism. Some parts of the BSTW are intruded by Permian pegmatites. An eclogite-facies Cretaceous metamorphism can be stated in the Prijakt Subgroup in the Schobergruppe which is also a pegmatite-intruded area. The northern parts of the BSTW which overlay the Penninic units exposed in the Tauern Window underwent a final Tertiary metamorphism.
- (4) The nappe units of the Saualpe (SA) to the SE of the Austroalpine domain are the area of the classical Cretaceous (Eo-Alpine) high pressure metamorphism with the formation of eclogites. Numerous intrusions of Permian pegmatites signal that there could also be relics of older metamorphic events. The SA also comprises units with an amphibolite facies Cretaceous metamorphism.

The case studies represent a section across the Alpine basement in space from northwest to southeast, and, in time, enclosing metamorphism from the Ordovician to the Cretaceous, with a focus on the Carboniferous and Permian events.

2.2. SEM-Based Automated Mineralogy (SEM-AM)

Automated mineralogical methods [28], based on a scanning electron microscope SEM Quanta 650-FEG-MLA by FEI Company (Hillsboro, OR, USA), equipped with Bruker Dual X-Flash energy dispersive spectrometers for chemical analyses, were applied to complete thin sections of garnet-bearing micaschists and gneisses. Electron beam conditions were set at 25 kV acceleration voltage and a 10 nA beam spot. A software package for mineral liberation analysis (MLA version 2.9.0.7 by FEI Company, Hillsboro, OR, United States) was used for the automated steering of the electron beam, for energy dispersive spectroscopy (EDS) identification of mineral grains, and the collection of numerous EDS spectra. Monazite and xenotime grains and their microstructural relationships within a distance of ~100 µm from the target grains were detected by a sparse phase search routine. The data were used to select monazite grains for Th-U-Pb age dating and mineral chemical analysis by the electron probe microanalysers (EPMA). The EDS spectral mapping routine (GXMAP) produces a narrow grid of ~1600 EDS spectra per mm² from garnet and biotite as phases of interest. For the classification of minerals and compositions in the SEM-AM measurements, identified reference EDS spectra were collected from matrix phases, and from defined parts of several garnet porphyroblasts (core-mid-rim). Reference spectra from garnet were generically labelled with the corresponding garnet Fe, Mg, Mn and Ca compositions. When the labelled spectra were arranged on a colour scale, semi-quantitative garnet zoning maps were established which could be compared to wavelength dispersive spectroscopy (WDS) element maps [27–29]. The GXMAP measurements of complete thin sections allowed for the selection of a few typical garnets out of dozens of porphyroblasts for quantitative WDS analysis and WDS element mapping with EPMA.

2.3. Microstructurally Controlled Geothermobarometry by EPMA

Mineral-chemical analyses of silicate minerals in micaschists were performed through time with various electron probe microanalysers CAMECA SX50 (CAMECA SAS, Gen-

neuvilliers, France), JEOL JXA-8900R,, JEOL JXA-8200, JEOL JXA-8230, JEOL JXA-8530F (JEOL Ltd. Akishima, Japan) at several institutions, using beam conditions of 15 kV, 20 nA and 2 μm , and the correction procedures supplied by CAMECA (Gennevilliers, France) and JEOL (Akishima, Japan) companies. Garnet zonations were analysed in detailed traverses. The compositions of associated feldspar and mica were documented by several single-point analyses. When thermodynamic equilibrium was assumed, two principal methods for estimating P-T conditions recorded in metamorphic rocks could be applied. Classical thermobarometry employs mineral-chemical compositions of phases involved in continuous cation-exchange and net-transfer solid-solid reactions [30,31]. Alternatively, pseudosection calculations can model phase assemblage stability fields for given bulk compositions and also allow the contouring of divariant fields [32]. Both methods have the basic pre-requisites and uncertainties of thermodynamic data in common. However, the pseudosection calculations involve an additional assumption concerning the effective local chemical bulk composition in a rock domain [32]. By this method, a rock bulk composition is related to P-T conditions. Compositional layering, strong variations in modal mineralogy and highly variable distribution of garnet in combination with several zoned porphyroblast generations imply significant compositional heterogeneities in metapsammopelites. The unknown sizes of the involved rock domain(s) impose uncertainty upon the effective local reactant bulk composition(s) for pseudosection calculations. Therefore, classical thermobarometry was chosen as the preferred method.

The geothermobarometric calculations require the combinations of mineral-chemical analyses from garnet, mica and plagioclase in equilibrium. Microstructural observations and the chemical evolution of the mineral phases provided criteria for the definition of local equilibria [33,34]. Traverses across garnet porphyroblasts may not have passed the entire core region and porphyroblasts may display zonation gaps. Some garnets may show only a part of the complete garnet chemical evolution in a sample. Such complications are not necessarily evident by the zonation profiles alone but can be checked in grossular-pyropes-spessartine coordinates. When garnet is the main Mn fractionating phase, its Mn content during crystallisation is controlled by Rayleigh fractionation [30]. This allows to recognize the relative temporal chemical growth evolution of the porphyroblasts. For each sample, a characteristic garnet mineral-chemical evolution trend can be derived from a compilation of the single-core-rim zonation profiles in grossular-pyropes-spessartine coordinates. Selected analyses out of the garnet chemical evolution trend in the ternary diagrams could then be used for thermobarometry. The main foliation (S_2) in metapelites by phyllosilicates and long prismatic minerals such as kyanite or fibrolitic sillimanite is related to a later deformation stage as it surrounds mm-scale microlithons with garnet, feldspar, mica, staurolite, aluminosilicates and quartz. Curved and planar internal foliations S_{1i} in porphyroblasts represent an early stage of deformation. External and internal structures of syn- and intertectonic garnet porphyroblasts were interpreted as successive incremental steps of progressive deformation [35]. The internal porphyroblast- S_{1i} to the external matrix- S_2 relationships allowed to establish the relative time of crystallisation. This enabled to relate the mineral-chemical data from mica and plagioclase to the garnet mineral-chemical evolution trends [33–35]. For the geothermobarometric calculations, mica and plagioclase of S_{1i} in garnets were related to early stages, and syn- S_2 mica and plagioclase to later stages of garnet growth. Inclusions in different core, intermediate and rim sites were assigned to the corresponding parts of the garnet porphyroblasts. When garnet had no inclusions, cores of zoned plagioclase and S_1 -biotite within the same microlithon could be interpreted to be in equilibrium with the garnet core. Rims of plagioclase, unzoned plagioclase and S_2 -mica were correlated to the garnet rim [33,34].

Temperatures were estimated using garnet-biotite geothermometers. Pressures were calculated with the garnet-aluminosilicate-plagioclase-quartz (GASP) and the garnet-biotite-muscovite-plagioclase (GBMP) geobarometers. Recalculations of P-T data were performed with the recent empirical re-calibration of the GBMP barometer [36]. The geothermobarometric estimates include a minimum error of ± 50 °C and ± 1 kbar. Un-

certainties about P-T paths calculated from the zoned garnets arose from quantitative systematic error in microprobe analyses and thermodynamic data. Shapes or the relative $\Delta P/\Delta T$ trends of P-T paths appeared to be mainly preserved when the uncertainties about corresponding plagioclase and mica were considered [30,34].

This concept of relating the chemical evolution of minerals during progressive shearing deformation to the P-T evolution was successfully applied to metapelites which underwent a single metamorphic cycle [30,33,34]. In the basement of the Alps already metamorphosed rocks were overprinted by second metamorphic cycles at various degrees. In such cases, the foliation generated during the early metamorphism would be re-activated and overprinted during the later metamorphism. The major pre-existent planar anisotropy of the rocks, given by the mica-rich foliation planes, simply accommodates the strain during the second metamorphic cycle. Dependent on the intensity of deformation, a heterogeneous overprint along distinct zones, leaving microlithons with preservation of structural relics, or a complete homogeneous transformation can be expected. In the Aiguilles Rouges Massif and the Austroalpine Saualpe basement, such heterogeneous overprint is obvious in foliation-parallel fine-grained high-temperature mylonitic layers of high strain with variable mm-to-dm thickness [29]. Mica compositions would only slightly change during recrystallisation and plagioclase would show further zonations and porphyroblast generations. Thus, chemical zonations of garnet would provide the best criterion for recognition of a second metamorphic cycle. Mn-rich garnet, which crystallised during the first metamorphic cycle, would undergo heterogeneous resorption along the rims. During the second metamorphic event, garnet with Mn-poor compositions would overgrow the older porphyroblasts or crystallise in a distinct new porphyroblast generation [27,29].

2.4. Chemical Th-U-Pb Monazite Dating by EPMA

Th-U-Pb dating of monazite by electron probe microanalysis (EPMA) is based on the given fact that common Pb in monazite (LREE, Th)PO₄ is negligible compared to radiogenic Pb resulting from the decay of Th and U [9]. Analysis of the bulk Th, U and Pb concentrations in monazite by EPMA, at a constant ²³⁸U/²³⁵U, allows for the calculation of an isochron age and/or for single-domain ages with a considerable error [9–11,37–39]. Monazite analyses were performed with instruments JEOL JXA-8200, JXA-8530F and JXA-8230 (JEOL Ltd., Akishima, Japan) with individually adopted analytical protocols [40,41]. Potential problems of data comparability were avoided by using the same reference monazite, labelled as Madmon, with validated special ThO₂*-PbO characteristics [40] for offline re-calibration of ThO₂, and for the data control by repeated measurements during the analytical sessions with each instrument. The electron beam was set at 20 kV acceleration voltage, 50 nA beam current for calibration, 100 nA beam current for measurements and 5 μm beam diameter. The Mα1 lines of Th and Pb and the Mβ1 lines for U of PETH or PETL crystals in spectrometers with a capsuled Xe-Ar proportional counter were chosen for monazite analysis. Natural crocoite or vanadinite were used for calibration of Pb. The U was calibrated either on a glass standard with 5 wt% UO₂ or on U metal. Calibration of Th on metal turned out to be problematic due to oxidization; therefore, monazite Madmon with ~12 wt% ThO₂ was preferably used for calibration of all measurements. Calibrations of rare earth elements (REE) were performed with the orthophosphates with negligible Pb from the Smithsonian Institution [42]. Counting times of 320 s (Pb), 80 s (U) and 40 s (Th) on peak were utilised. Interference of YLg on the PbMa line was corrected by linear extrapolation of correction factors gained from analysis of various Y-bearing standards [9]. The interference of the ThMg line on the UMb line was also corrected. A 1σ error deduced from the counting statistics (error derived from JEOL software) and an error $\epsilon_{Pb} = \sqrt{(Cts/s_{PEAK} + Cts/s_{BKG}) / (Cts/s_{PEAK} - Cts/s_{BKG})}$ based on the counting statistics in counts per second on the peak (PEAK) and background (BKG) spectrometer positions were propagated to an error in Pb element %. For measurements of Pb on JEOL-JXA-8200 (JEOL Ltd., Akishima, Japan), the error in element% was ~0.008 for the given dwell time (recalculated from the JEOL software), or ~0.003 (recalculated from

ε_{Pb}) for the reference monazite (Madmon) which contained ~0.25 wt% Pb. The larger error value in Pb element% of 0.008 was applied to these analyses, which propagated for the reference monazite Madmon with ~506 Ma typically to ± 40 Ma (2σ), and for Permian monazites (~0.04–0.08 wt% Pb) to 70–90 Ma (2σ). For Pb measurements with the JEOL JXA-8530F and the JEOL JXA-8230, the error in element% was ~0.004 (recalculated from the error given by JEOL software), or ~0.001 (recalculated from ε_{Pb}) for the reference monazite Madmon. We applied an error in Pb element% of 0.003 to all these analyses, which propagated for the reference monazite Madmon with ~506 Ma typically to ± 12 Ma (2σ), and for Carboniferous monazites (~0.085 wt% Pb) to 20–30 Ma (2σ). All monazite measurements with the various EPMA instruments reported here referred to the same reference monazite Madmon. The number of single analyses varied with the grain size of the monazites, e.g., 1–2 analyses in grains of < 40 μm and ~10 analyses on grains of 100 μm diameter. In the first step, the monazite chemical ages were calculated using the methods of [9]. In the second step, monazite ages were determined using the ThO_2^* -PbO isochrone method (CHIME) of [10] where ThO_2^* was the sum of the measured ThO_2 plus ThO_2 equivalent to the measured UO_2 . This age corresponded to the slope of a regression line forced through zero in ThO_2^* vs. PbO coordinates. Calculation of the regression line provided an underestimation of the error. Therefore, in the third step, the weighted average ages for monazite populations were calculated from the single analyses which defined the regression line [43]. When a large monazite allowed several analyses, the weighted average ages were also calculated from the ages of single analyses. Mostly, the sizes of monazite grains were below 50 μm . In consequence, it was intended to perform a narrow grid of full quantitative analyses from such grains. In general, the isochrone ages and weighted average ages of monazite populations coincided within the error. The age data were interpreted as the time of closure for the Th-U-Pb system in monazite during growth or recrystallisation in the course of metamorphism.

3. Results from Garnet- and Monazite-Bearing Metapsammopelites

3.1. Aiguilles Rouges External Massif (European Plate)

The Aiguilles Rouges Massif, one of the External Massifs in the Helvetic Domain (Figure 1a,b), is mostly preserved from intense Alpine tectonic and metamorphic overprint, attaining only the lowest greenschist facies grade. The massif is composed of metapelites and metagreywackes, diopside marbles, orthogneisses, garnet amphibolites, migmatites, eclogites, meta-ultrabasites and granulites. Zircon and monazite dating mainly gave Carboniferous ages [44,45]. Early Paleozoic protolith ages of magmatic rocks also came into discussion [46]. The typical pre-Mesozoic basement was observed between the Lac Cornu and Col de Bérard regions. An impressive, tilted discordance between the metamorphic basement and overlying Triassic sediments was exposed. A high temperature mylonitic garnet gneiss at locations AR1890 and AR40 had a fine-grained foliated matrix surrounding lens-like microlithons with large broken garnet porphyroblasts of up to 1.5 cm in diameter. The other samples were garnet micaschists from a western series and from an eastern part of the sequence [47]. Typical microstructures of multistage metamorphism were observed from monazites [48]. These were the late partial decomposition of Carboniferous monazite to apatite (Figure 2a), and the satellite structure (Figure 2e,f).

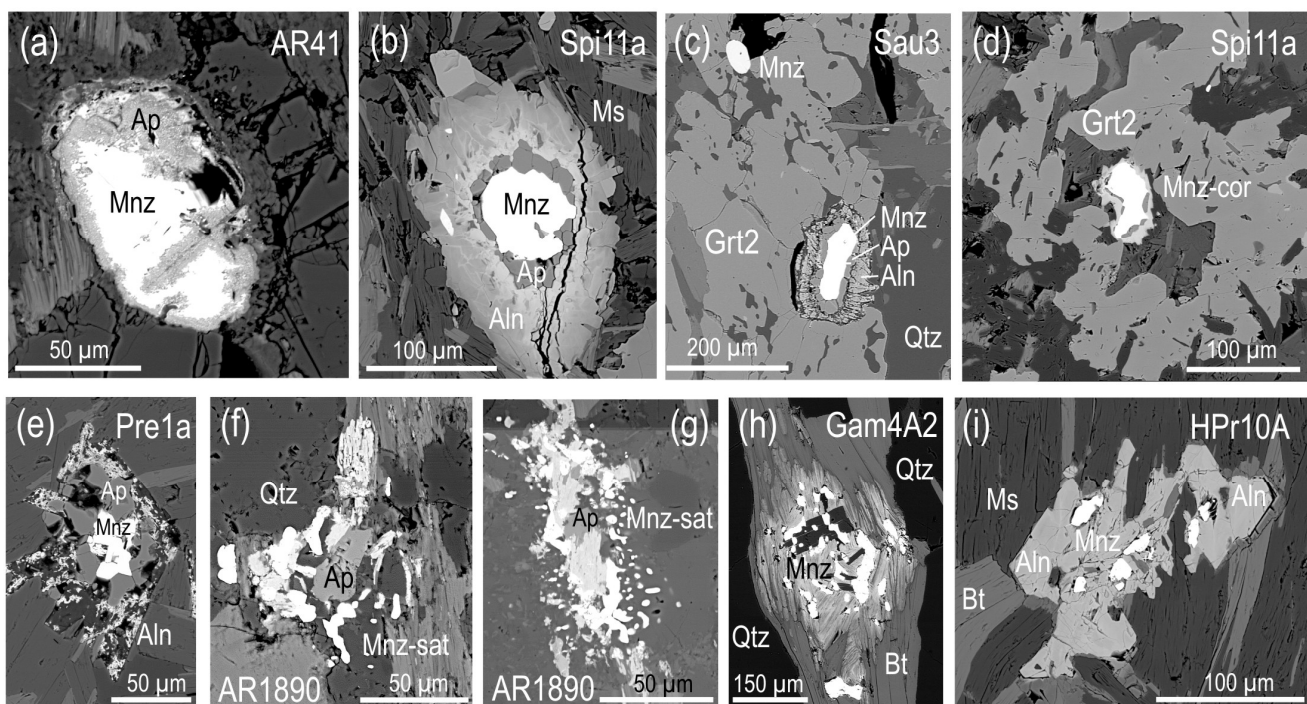


Figure 2. Microstructures of monazite in backscattered electron images (BSE). (a) Partial and graded decomposition of Carboniferous monazite (Mnz) to apatite (Ap) in the Aiguilles Rouges Massif. (b) Permian monazite with small apatite (Ap) and broad rim of allanite (Aln), initial stage of corona structure (Saulpe Micaschist Complex). (c,d) Corona structure around Permian monazite (Mnz-cor) enclosed in garnet (Grt) in contact to quartz (Qtz), suggesting a Cretaceous age of garnet (Saulpe Eclogite and Micaschist complexes). (e) Permian monazite with broad apatite rim and few tiny allanite crystals in the outer corona (Saulpe Preims Complex). (f,g) Monazite satellite microstructures (Mnz-sat) with Carboniferous ages around apatite in mylonitic garnet gneiss (Aiguilles Rouges Massif). (h) Cluster microstructure of Carboniferous monazite in biotite (Bt) in the Oetztal-Stubai Complex. (i) Cluster structure of Cretaceous monazite in allanite (BSTW, Prijakt Subgroup).

Garnet compositional profiles were flat in the cores with up to 30% pyrope and low spessartine and grossular (<2%) contents in the mylonitic garnet gneisses. Toward the garnet rims, a decrease in pyrope and increase in grossular were observed. Such garnet zonation profiles are typical of homogenisation of cores by diffusion at high temperature and resorption of the rims during retrogression [30]. Thermobarometric calculations from the mylonitic garnet gneisses indicated that the Mg-rich homogenized garnet cores crystallized at 6 kbar/800 °C. From the zoned garnet rims, it was possible to calculate 3 kbar/650 °C (Figure 3a). P-T data from both analysed samples overlapped within error [47]. Garnet in the micaschists displayed growth zonations with a considerable decrease in spessartine (Mn) contents from cores to rims, while pyrope (Mg) increased (Figure 3b–d). Following the garnet zonation, trends from the western series maximal temperatures of 7 kbar/670 °C were calculated. Calculations from garnet rims and inner parts gave 500 to 600 °C between 11 and 6 kbar which were arranged along a prograde–retrograde P-T path along decreasing pressures. The P-T data from the western series were completed by 13 kbar/650 °C, calculated from garnet and enclosed clinopyroxene and 6 kbar/630 °C from amphibole equilibria in an amphibolitised eclogite [47]. This contrasted maximal temperatures around 7–8 kbar/600 °C along a decompression path in the micaschists to the east (Figure 3a).

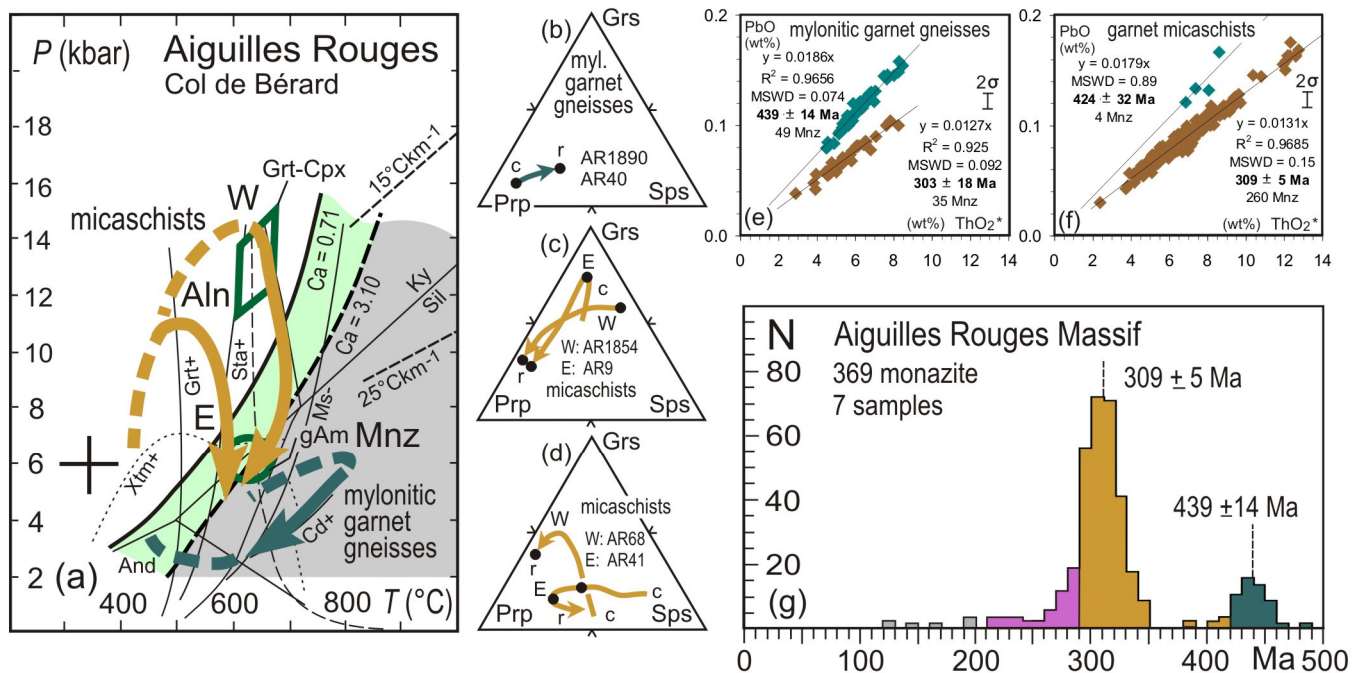


Figure 3. P-T paths, garnet zonation and EPMA Th-U-Pb monazite ages in the Aiguilles Rouges Massif (External Massif, Helvetic Domain). (a) P-T paths by microstructurally controlled geothermobarometry from garnet core-to-rim zonation in micaschists and paragneisses in the west (W) and the east (E) of studied area [47]. Aluminosilicates (and Ky, Sill), cordierite-in (Cd+), muscovite-out (Ms-) and staurolite-in and -out (Sta+, Sta-) univariant lines [30]. Stability fields (green and gray) of monazite (Mnz) and allanite (Aln) at different bulk rock contents as a function of Ca wt%; xenotime (Xtm) stability field. Bold cross marks uncertainty of ± 50 °C/ ± 1.0 kbar on P-T estimates. Geothermobarometric data from amphibolitized eclogite with garnet-clinopyroxene (Grt-Cpx) and from amphibolite with green amphibole endmember (gAm) equilibria are marked in green. (b–d) Grossular-pyropo-spessartine (Grs-Prp-Sps) ternary diagrams of garnet core-to-rim (c, r) zonation, colors of arrows are related to the P-T paths in (a). (e,f) ThO₂*-PbO (wt%) isochrone diagrams. ThO₂* is ThO₂+UO₂ equivalents expressed as ThO₂. General minimal 2 σ error on monazite PbO analysis is shown by a bar. Regression lines of monazite populations marked by colours give a coefficient of determination R² and were forced through zero [9,10]. Weighted average ages in Ma with MSWD and minimal error of 2 σ were calculated from the single analyses belonging to an isochrone [43]. The coloured symbols mark analyses belonging to monazite age populations and defining isochrones, falling into Ordovician-Silurian (blue-green) and Carboniferous (brown) ranges of ages. (g) Histogram of monazite ages.

Two distinct generations of ages were revealed by EPMA monazite dating in the mylonitic garnet gneisses. An older group with ages at 439 ± 14 Ma was found in large matrix monazite grains next to the garnet porphyroblasts. Monazite enclosed in garnet exclusively displayed Ordovician-to-Silurian ages. In some of the larger matrix grains, several marginal analytical points also yielded Carboniferous ages [47]. Exclusively Carboniferous ages occurred in multigrain aggregates of monazites with small grain sizes aligned along the mylonitic foliation and in some cases in satellite microstructures around apatite (Figure 2e,f). In the ThO₂*-PbO diagrams, the Ordovician-to-Silurian and Carboniferous monazite ages appeared along two distinct isochrons and separated the maxima in the histogram (Figure 3e–g). There were no monazite analyses with intermediate ages in between these groups.

Carboniferous monazites dominated in the micaschist samples (Figure 3f). Only a few single analyses in the cores of the matrix grains with sizes of 10–40 μ m provided the Ordovician-to-Silurian ages and were interpreted as metamorphic relics. Monazites enclosed in garnet were also of Carboniferous age, but appeared as slightly older (~330 Ma) than monazites (~312 Ma) in the matrix. The Ordovician-to-Silurian monazites had a much higher Y₂O₃ (~3.2 wt%), whereas the maximal Y₂O₃ in the Variscan monazites was only 1.5 wt% [47].

3.2. Oetztal-Stubai Complex in the Western Austroalpine Basement

The Oetztal-Stubai Complex (OSC) to the west of the Tauern Window can be attributed to the Oetztal-Bundschuh nappe system [1]. Monotonous sequences of paragneisses and micaschists with sparsely interlayered thin marbles and metabasites dominate the complex [13,49]. In the Oetztal valley, the 8 km-thick Central Metabasite Zone (CMB) is exposed. Protoliths of the Central Metabasite Zone are gabbros and basalts with MORB chemistry and Early Cambrian ages, emplaced in a back-arc setting [50]. Acid orthogneisses with S- and I-type affinity are interlayered with the metapsammopelitic sequences. In general, Ordovician protolith ages have been recognised for these rocks by various dating methods [13,21,51].

The OSC is the classical area of polymetamorphism in the Alps [6–8,21]. Various isotopic dating methods have been developed and applied there. An Early Paleozoic high-temperature anatectic event was reported from the Winnebach, Verpeil and Klopaier migmatites [21,52,53]. Eclogite-facies and amphibolite-facies conditions were attained during the Carboniferous metamorphism [50,54]. A Carboniferous metamorphic overprint resulted in kyanite, sillimanite and andalusite mineral zones of which boundaries cut across and postdate large-scale Schlingen structures of a regional foliation [55]. An increasing grade of a Cretaceous overprint towards the south has been described [7,8]. This is obvious from Carboniferous-to-Cretaceous K-Ar and Rb-Sr “mixed ages” of mica, changing to Cretaceous ages towards the SE. The successive occurrence of chloritoid and then staurolite towards the Schneeberg and Texel Complexes accompanied by distinct growth zones in garnet porphyroblasts were also assigned to this Cretaceous (Eo-Alpine) overprint [56,57]. The chloritoid and staurolite isograds and the NW boundary of biotite ages of the Cretaceous metamorphism were also discordant to the Schlingen structures.

In the Sellrain region, micaschists contain large garnet porphyroblasts which enclose staurolite. Staurolite occurs also with kyanite and sillimanite in the foliated matrix. A late generation of staurolite and kyanite crystallized across the main foliation S_2 [58]. The Central Metabasite Zone (CMB) with occurrences of eclogites extends towards the E and metabasites alternate there with metapsammopelites in the Alpeiner Valley in the Stubai region. The general mineral assemblage in these micaschists is quartz, plagioclase, muscovite, biotite and garnet. Garnet porphyroblasts are accompanied by staurolite and kyanite which are partly sericitised in the foliated matrix. Garnet encloses staurolite in its rims [41,58]. To the S of the CMB, around the Hochstubaihütte to the E of Sölden, in garnet micaschists the kyanite is the prevailing aluminosilicate. A significant retrogressive overprinting of the metapelites is obvious from abundant chlorite replacing garnet and biotite and the pseudomorphic replacement of kyanite and staurolite by aggregates of sericite. Sometimes a (re)-crystallisation of muscovite is observed within these pseudomorphs [58].

Garnets in the metapelitic assemblages crystallized during the formation of the main foliation S_2 . The porphyroblasts displayed growth zonations with low pyrope contents in the cores and pyrope-rich rims, while Mn decreased and Ca increased and then decreased (Figure 4a–d). A prograde metamorphism along a clockwise P-T path with high pressure amphibolite-facies peaked pressure conditions at 11–13 kbar and peaked temperature conditions at ~680 °C, and a post P_{max} path with decompression to 5 kbar near 700 °C was estimated from the micaschists. The P-T paths from the Stubai area matched the P-T paths described from micaschists in the Sellrain, Umhausen and Sölden areas [41,58]. The maximal pressures calculated from the micaschists were slightly lower than the conservative pressure estimates by the garnet-clinopyroxene equilibria from eclogites. Other estimates, based on phengite equilibria and thermodynamic data, at around 27 kbar, were afflicted by the assumption of low water activity. They were not confirmed by the observation of coesite or relics of it [50]. P-T estimates from amphibolites matched the retrograde sections of the P-T paths (Figure 4a).

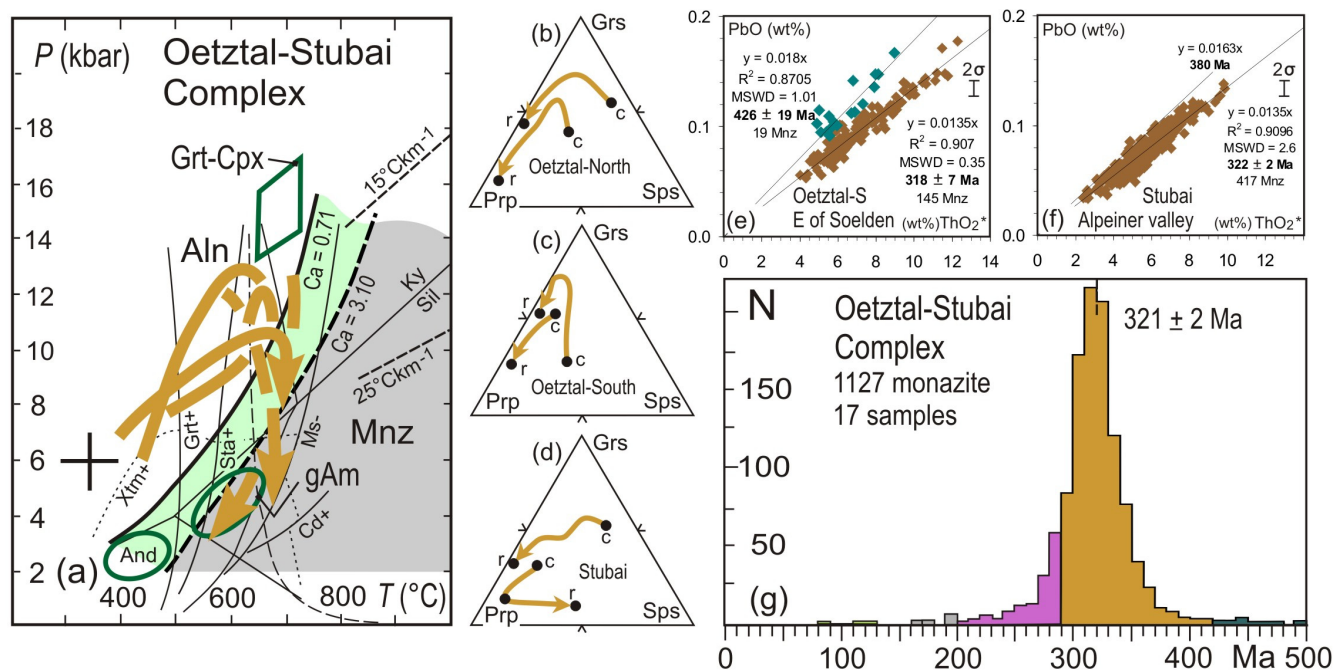


Figure 4. P-T paths, garnet zonation and EPMA Th-U-Pb monazite ages in the Oetztal-Stubai Complex in the Austroalpine Domain. (a) P-T paths by microstructurally controlled geothermobarometry from garnet core-to-rim zonation in micaschists and paragneisses in the northern and southern parts of studied area [41,58]. Aluminosilicates (and Ky, Sill), cordierite-in (Cd+), muscovite-out (Ms-) and staurolite-in and -out (Sta+, Sta-) univariant lines [30]. Stability fields (green and gray) of monazite (Mnz) and allanite (Aln) at different bulk rock contents as a function of Ca wt%, and with the xenotime (Xtm) stability field. Bold cross marks uncertainty of ± 50 °C/ ± 1.0 kbar on P-T estimates. Geothermobarometric data from amphibolitised eclogite with garnet-clinopyroxene (Grt-Cpx) and from amphibolite with green amphibole endmember (gAm) equilibria are marked in green (b–d) Grossular-pyropes-spessartine (Grs-Prp-Sps) ternary diagrams of garnet core-to-rim (c, r) zonation, colors of arrows are related to the P-T paths in (a). (e,f) ThO₂*-PbO (wt%) isochrone diagrams. The coloured symbols mark analyses belonging to monazite age populations and defining isochrones, falling into Silurian (blue-green) and Carboniferous (brown) ranges of ages. (g) Histogram of monazite ages.

For presentation in ThO₂*-PbO diagrams, the samples to the S of the CMB from the region W of Soelden and from the Stubai regions were selected (Figure 4e,f). The weighted average ages of large single grains ranged around 330–320 Ma. In three samples, one observes a non negligible number of monazites with Silurian ages, matching observations from migmatite locations [53]. These pre-Carboniferous ages were interpreted as the relics of an older monazite generation. Monazite in microstructures of clusters (Figure 2c) were somewhat younger as the overall isochrone [41]. In these samples, it was possible to define minor populations of younger monazites showing Permian isochrones at 284 ± 6 and 276 ± 7 Ma. The Permian-age monazites were always single analyses within grains of the Carboniferous age. They were interpreted to signalize a discernible post-Variscan thermal overprint or slow cooling during Permian times [41,58]. Isochrones with Carboniferous ages clearly prevailed. In the histogram view, there were unimodal distributions around the Carboniferous isochrone ages (Figure 4g). A search for monazite in micaschists immediate to the north of the Schneeberg Complex was not successful. There is yet no report of Cretaceous monazite ages, although sampling locations are within the metamorphic aureole of Cretaceous chloritoid and mica ages [41,53,58].

3.3. Basement to the South of the Tauern Window and Related Units

The Austroalpine basement to the south of the Tauern Window (BSTW) is located between the underlying Penninic unit, and the Periadriatic Lineament (Figure 1a,c). According to the classification of Alpine nappes, the northern part of the BSTW belongs to the Koralpe-Wölz nappe system, whereas the parts to the south of the Deferegggen-Antholz-Vals Line

(DAV) belong to the Drauzug–Gurktal nappe system [1]. The northern part comprises the Northern-Deferegggen-Petzeck Group (NDPG), considered as the structurally lowermost unit. It is composed of micaschists, two-mica gneisses, biotite paragneisses, metaquartzites and some marbles. Several subgroups based on the association with metabasites can be distinguished. The structurally lowermost sequence is the Rotenkogel Subgroup, which contains hornblende gneisses with volcanic arc basalt geochemical signatures and 550–533 Ma protolith crystallisation ages [16]. Amphibolites, with MORB to within-plate basalt geochemical fingerprint, yielded a Pb-Pb zircon evaporation crystallisation age of 430 ± 2 Ma. In the Schobergruppe mountains, the Prijakt Subgroup is exposed in a structurally high position within the NDPG and bears amphibolitised eclogites with N-MORB-type geochemical characteristics and a Pb-Pb zircon evaporation protolith age of 590 ± 4 Ma [16]. The Prijakt Subgroup also encloses hornblende gneisses with Cambrian protolith ages, and acid orthogneisses with Ordovician protolith ages. The Deferegggen Group (DG) has a pre-Early Ordovician deposition age, as it was intruded by numerous metagranitoids with an S- and I-type affinity with Ordovician crystallisation ages [16]. The structurally overlying Thurntaler Phyllite Group (TPG) has a post-Early Ordovician depositional age, as it comprises intercalated acid volcanic rocks with Ordovician protolith ages [13,16]. The Oligocene Deferegggen-Antholz-Vals Line (DAV) separates the northern part with Cretaceous to Tertiary mica cooling ages from the Deferegggen Group and the Thurntaler Phyllite Group to the south where Carboniferous mica cooling ages prevail [59,60]. The latter signal a pre-Alpine metamorphism and only a minor and brittle Alpine overprint [16]. Alpine metamorphism hardly exceed $300\text{ }^{\circ}\text{C}$ in Triassic carbonate rocks of Kalkstein, Staller Alm and Zwischenbergen along the late-Alpine faults [16].

To the S of the DAV, the metapelites and Ordovician granitoids of the Deferegggen Group underwent a shearing deformation which produced isoclinal and sheath folds F_2 as well as the main foliation S_2 . Linear-planar fabrics in the Ordovician granitoids, now orthogneisses, are parallel to S_2 . The S_2 was refolded and overprinted at all scales by open to tight folds and crenulations F_3 . F_3 folds with steeply plunging axes are minor structures of large-scale syn- and antiforms labelled as Schlingen structures [16]. Toward the east and south of the region with Schlingen in the Deferegggen Group, the orientation of the F_3 fold axes grades from the steeply plunging direction into gentler WSW or ENE plunging. In the Thurntaler Phyllite Group, similar orientations of linear-planar fabrics and of later F_3 fold axes as in the adjacent Deferegggen Group were observed [16]. In micaschists the deformation with the formation of S_2 and F_3 was accompanied by the crystallisation of the strongly zoned garnet with microstructures of syncrystalline rotation. Kyanite and staurolite crystallised subsequent to garnet. Geothermobarometry yielded complex prograde P-T paths. Spessartine-rich garnets recorded the onset of shearing under increasing high-pressure low-temperature conditions of 7 kbar/ $380\text{ }^{\circ}\text{C}$ [61]. Then, followed isothermal decompression from 9 kbar to 5 kbar/ $500\text{ }^{\circ}\text{C}$ and subsequent recompression/heating during continuing shearing to 12 kbar at $650\text{ }^{\circ}\text{C}$, and further increasing temperatures up to $680\text{ }^{\circ}\text{C}$ accompanied by decompression (Figure 5a,e). The EPMA Th-U-Pb monazite dating of micaschist samples from the Deferegggen Group yielded single Carboniferous isochrons at 309 ± 9 Ma (sample 431), 308 ± 12 Ma (sample 750) and 307 ± 15 Ma (sample 839) which can be combined to a unimodal distribution around 309 ± 7 Ma (Figure 5i).

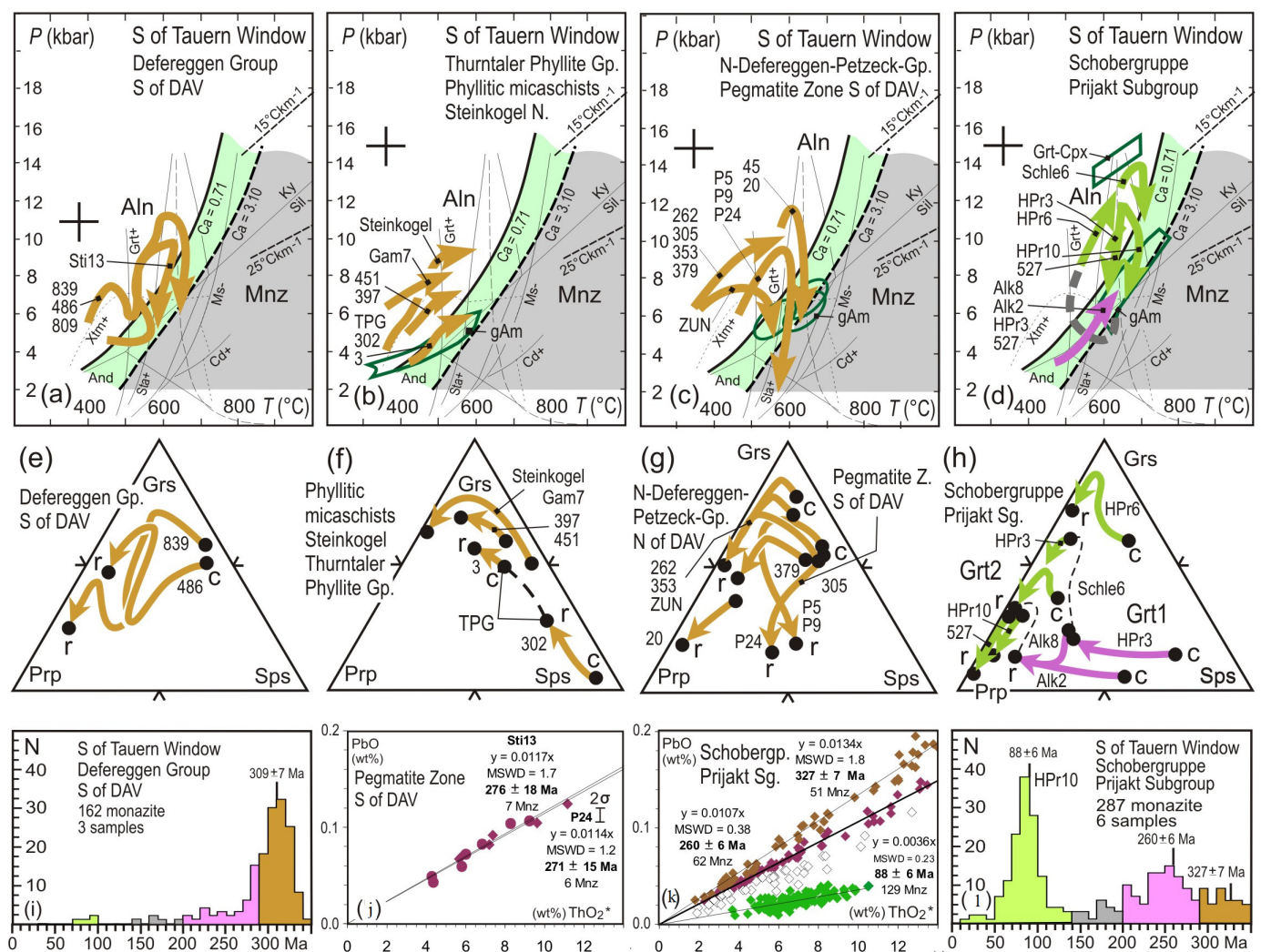


Figure 5. P-T paths, garnet zonation and EPMA Th-U-Pb monazite ages in various parts of the basement south of the Tauern Window in the Austroalpine Domain. Gp.: Group; Sg.: Subgroup; Z.: Zone. (a–d) P-T paths by microstructurally controlled geothermobarometry from garnet core-to-rim zonation in micaschists and paragneisses [16,61–63]. Aluminosilicates (and Ky, Sill), cordierite-in (Cd+), muscovite-out (Ms-) and staurolite-in and -out (Sta+, Sta-) univariant lines [30]. Stability fields (green and gray) of monazite (Mnz) and allanite (Aln) at different bulk rock contents as a function of Ca wt%, and with the xenotime (Xtm) stability field. Bold cross was uncertainty of ± 50 °C/ ± 1.0 kbar on P-T estimates. Geothermobarometric data from amphibolitised eclogite with garnet-clinopyroxene (Grt-Cpx) and from amphibolites with green amphibole endmember (gAm) equilibria. (e–h) Grossular-pyropes-spessartine (Grs-Prp-Sps) ternary diagrams of garnet core-to-rim (c,r) zonation, related to P-T paths in (a–d). (i) Histogram of monazite ages in the Defereggeng Group to the South of the Defereggeng-Antholz-Vals Line (DAV). (j,k) ThO₂*-PbO (wt%) isochrone diagrams. Data from zone with pegmatites immediate to the south of the DAV line and from the Prijakt Subgroup of the Schobergruppe. The coloured symbols mark analyses belonging to monazite age populations and defining isochrones, falling into Carboniferous (brown), Permian (violet) and Cretaceous (green) ranges of ages. (l) Histogram of monazite ages in the Prijakt Subgroup of the Schobergruppe.

Phyllitic micaschists occur in the upper part of the Defereggeng Group in a lithological transition to the overlying Thurtaler Phyllite Group [16]. Assemblages with garnet, biotite, muscovite, oligoclase, quartz and lacking staurolite and aluminosilicates were observed. The garnet showed increasing pyrope contents at high grossular contents from cores to rims. Maximal pressure and temperature of the prograde P-T paths were at 8 kbar/520 °C (Figure 5b,f). Similar garnet zonation, and similar prograde P-T paths reaching maximal conditions of 8 kbar/530 °C, were observed from the Steinkogel Nappe (SN) which overlies the Innsbrucker Quartzphyllite to the N of the Tauern Window (Figures 1c and 5b,f). A

monazite suitable for EPMA Th-U-Pb dating has not yet been detected in the samples from the phyllitic micaschists.

The Thurntaler Phyllite Group overlies the Deferegggen Group along a partly over-turned pre-Alpine foliation-parallel contact. Quartzphyllites and phyllitic micaschists are interlayered by amphibolites, epidote amphibolites, chlorite schists, quartzites, graphite phyllites and rare marbles (Figure 1c). Assemblages with garnet, biotite, muscovite, oligoclase, quartz and lacking staurolite and aluminosilicates were observed and the maximal P-T conditions calculated from Mg-rich garnet rims were 6 kbar/560 °C. These conditions of an epidote amphibolite facies metamorphism were confirmed by assemblages in metabasites with strongly zoned magnesio-hornblende and tschermakite with albite, oligoclase, epidote, chlorite, titanite and quartz, which crystallized at increasing temperatures from 2.5 kbar/300 °C up to 6 kbar/600 °C/6 kbar (Figure 5b,f). Identical mineral assemblages, amphibole mineral chemical compositions and P-T conditions have been found in amphibolite samples from the western parts of the Kreuzeck Phyllite Group [16]. A monazite suitable for EPMA Th-U-Pb dating has yet not been detected in the samples from the Thurntaler Phyllite Group.

In the lower part of the Deferegggen Group, which crops out immediate to the south of the DAV line, the micaschists are intruded by numerous pegmatite bodies. A distinct zone with micaschist-bearing fibrolitic sillimanite is developed in the host rocks around the pegmatites. Fibrolitic sillimanite crystallized in the foliation planes and replaced the garnet. Porphyroblasts of andalusite and staurolite overgrew the foliation S_2 . Staurolite also encloses garnet. These microstructures indicate that the aluminosilicates are related to later stages of metamorphism and crystallized subsequent to garnet [16]. Garnet zonations in this pegmatite zone displayed a significant decrease in Ca towards the rims, corresponding to a prograde P-T evolution towards 10 kbar/600 °C followed by a marked decompression to 4 kbar/600 °C (Figure 5c,g). The EPMA monazite dating in the pegmatite zone to the south of the DAV [62] yielded Permian ages at isochrons of 276 ± 18 Ma (sample Sti13) and 271 ± 15 Ma (sample P24, Figure 5j).

To the north of the DAV and to the W of the Isel river, a polyphase metamorphic evolution was recorded. The increasing intensity of an Alpine structural overprint toward the Austroalpine-Penninic suture was not matched by any changes of the mineral chemistry in the garnet, biotite, muscovite, plagioclase and quartz-bearing metapelite assemblages or by changes within the garnet zoning profiles. Garnet zonations showed increasing pyrope contents from cores to rims, indicating a crystallisation at an increasing temperature and pressure. Thermobarometry of garnet metapelites gave no hints to metamorphic gradients related to this structural overprint. Maximal pressures ranged at 10–12 kbar and maximal temperatures were at 650 °C/7 kbar, connected by decompression paths as exemplified by samples 20 and 45 (Figure 5c,g). In combination with the structural observations, it was concluded that a greenschist-facies Tertiary overprint did not exceed the prevailing pre-Alpine amphibolite-facies metamorphic conditions [16,63]. The maximal thermal conditions of the regional metamorphic Alpine overprint were 500 °C at 4 kbar, calculated from amphibolites in the Penninic Upper Schieferhuelle. The contact metamorphism in the vicinity of the Oligocene Rieserferner intrusion reached maximal conditions of 3 kbar/620 °C, with the crystallisation of sillimanite, staurolite, andalusite and K-feldspar [16].

Amphibolitised eclogites were restricted to the Prijakt Subgroup in the Schobergruppe mountains to the E of the Isel river and to the Kreuzeckgruppe mountains. Pre-Alpine and Cretaceous ages for the eclogite formation have been discussed [64,65]. The Lu-Hf geochronology of garnet in eclogites allowed to identify major events, one with a 313 Ma minimum age reflecting for Carboniferous metamorphism, and a second event (104–97 Ma) related to a Cretaceous high pressure metamorphism in a Prijakt Subgroup amphibolitised eclogite body [66]. The data confirmed Cretaceous EPMA Th-U-Pb monazite ages in micaschists [62]. Garnets in staurolite and kyanite-bearing micaschists in the vicinity of the amphibolitised eclogites displayed complex zonations [62,64]. A re-interpretation of these zonation profiles, following the findings in the Saualpe reported below, allowed to

conclude for two distinct metamorphic episodes. An early metamorphic episode led to the crystallisation of a Mn-rich and Ca-poor garnet one along a prograde P-T path from 3.5 kbar/460 °C to 6 kbar/600 °C. A late metamorphic episode with the crystallisation of a Mn-poor but Mg- and Ca-rich garnet two, partly in rims around garnet one, was characterised by various P-T segments. These involved prograde as well as prograde-retrograde paths which passed conditions at 14 kbar/680 °C. Garnet-clinopyroxene equilibria from eclogite garnets gave slightly higher pressures (Figure 5d,h). Monazite ages from the micaschists ranged around Carboniferous (327 ± 7 Ma), Permian (260 ± 6 Ma) and Cretaceous (88 ± 6 Ma) isochrons [62]. In most of the single samples, the Carboniferous and Permian monazite ages prevailed. Only in sample HPr10 with small, clustered monazite in allanite, the Cretaceous monazite ages were dominant (Figures 2h and 5d,k,l).

3.4. Saualpe Nappe Units

The Austroalpine Saualpe metamorphic complex (Figure 1c) was composed of five nappe units. The lowermost part was the parautochthonous amphibolite facies Kliening Complex. Toward the hanging wall followed the amphibolite facies Preims Complex and then the Eclogite Complex. An amphibolite facies Micaschist Complex, also labelled as the Plankogel Complex, marked the top of the metamorphic pile which was tectonically overlain by the lower greenschist facies Phyllite Complex [67]. A significant metamorphic break along a low-angle normal fault was observed between the Micaschist and the Phyllite complexes. Metamorphic breaks were further observed between the other complexes [67–70]. Meta-pegmatite layers and bodies, referred to as pegmatite gneiss, with K-feldspar, muscovite and tourmaline clasts, represented protoliths of Permian to Triassic ages, and were restricted to the Preims, Eclogite and Micaschist complexes. Permian and Cretaceous metamorphic events have yet to be demonstrated in the Preims and Eclogite complexes [2,24,27,29,67,70–72]. In the Kliening Unit, where no pegmatite gneisses occur, the Cretaceous mica and monazite ages were predominant [27,67].

The strong and partly mylonitic deformation of the pegmatite bodies implies a Cretaceous or Alpine age of the main foliation. These former Permian to Triassic pegmatites, as known from the Austroalpine basement in the southern part of the Oetzal-Stubai Complex and to the south of the Tauern Window [22,23], indicate a Paleozoic minimum sedimentation age of their host rocks in the Saualpe. This was supported by the zircon U-Pb dating of amphibolites in the Micaschist Complex which yielded Early Devonian magmatic protolith crystallisation ages [73]. Ordovician granitoids, which are widespread in other parts of the Austroalpine basement [4], did not occur.

Two garnet generations with monophase and polyphase porphyroblasts were revealed in metapelites from four Saualpe complexes. Garnet one had a uniformly decreasing Mn, low Ca and significantly increasing Mg from cores to rims in the four complexes. The geothermobarometry of garnet one assemblages signalled a crystallisation along a M1 prograde metamorphic P-T path culminating at 6 kbar/600–650 °C, followed by decompression (Figure 6a,b,e,f). Garnet two always displayed low Mn at high Ca and Mg. The grossular was increasing and then decreasing, while pyrope was decreasing and then increasing toward the rims. The garnet two assemblages recorded a prograde P-T path from 8 kbar/530 °C/ to 10–13 kbar/700 °C for metamorphism M2 in the Kliening Complex, and from 10–12 kbar/620 °C to 14–15 kbar/700 °C for M2 in the Preims Complex [27]. In the micaschists of the Eclogite Complex, garnet two displayed first an increasing grossular at a decreasing pyrope, then an increasing grossular and pyrope, and, finally, a decreasing grossular with an increasing pyrope, always at high Ca and Mg and low Mn. (Figure 6c,g). This recorded a P-T evolution for M2 which passed through eclogite-facies conditions and reached maximum temperatures at 14 kbar/~750 °C during decompression-heating [29]. Maximal pressure conditions for M2 could be estimated at around 22 kbar and matched conservative estimates from garnet-clinopyroxene equilibria in the eclogites [70,71]. In the Micaschist Complex, the zonations in garnet two porphyroblasts allowed the calculation of a prograde-retrograde P-T path segment for M2 with maximal pressure conditions at

around 14 kbar/620 °C (Figure 6d,h). When the maximal pressures for the M2 event were compared for samples situated next to the nappe boundaries, it was evident that a major discontinuity with an inverse character existed between the Preims and Eclogite complexes, and with a normal character between the Eclogite and Micaschist complexes, as outlined in earlier studies [27,29,67–71].

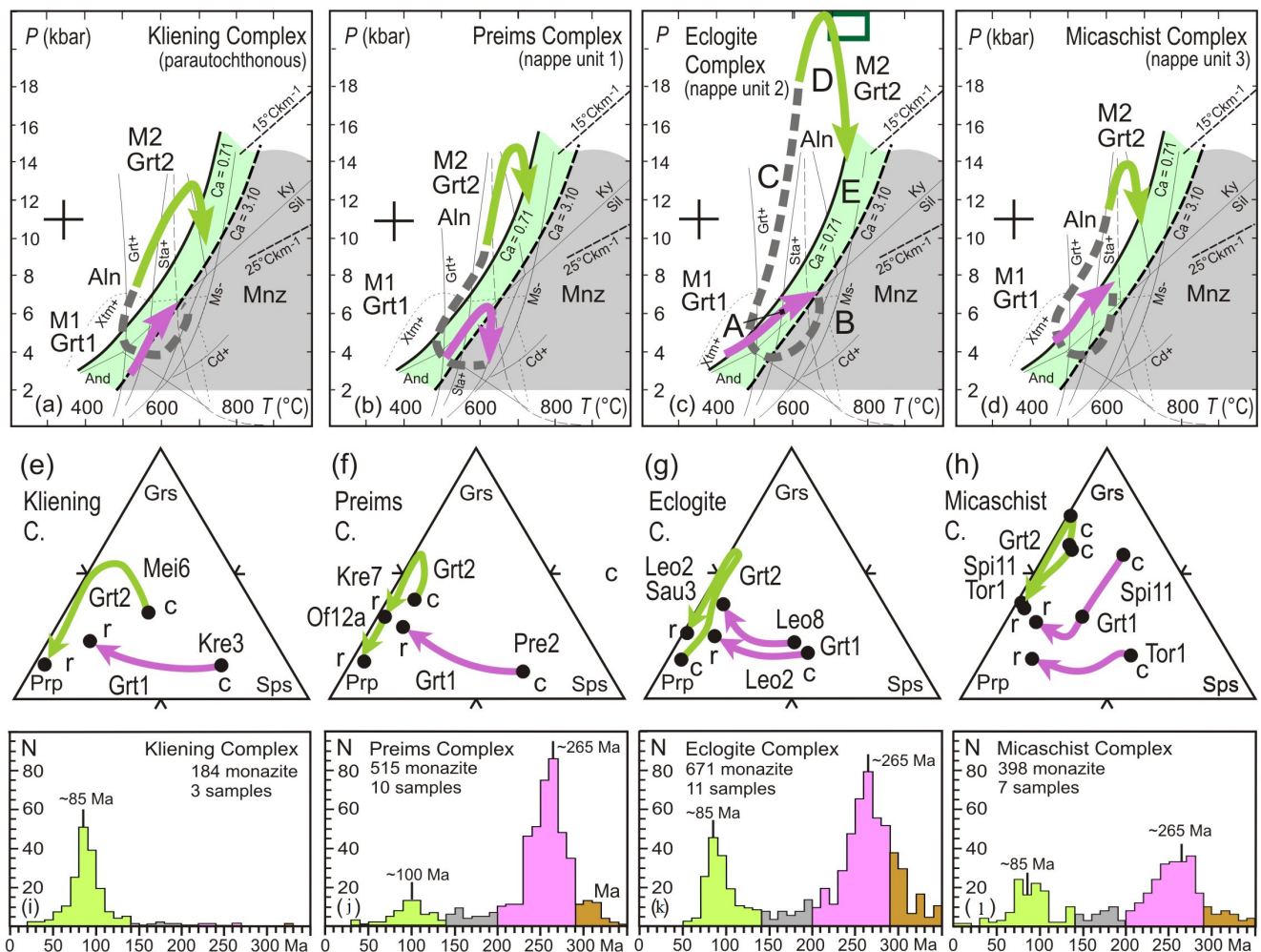


Figure 6. P-T paths, garnet zonation and EPMA Th-U-Pb monazite ages in the complexes of the Saualpe nappe stack in the Austroalpine Domain. (a–d) P-T paths by microstructurally controlled geothermobarometry from garnet core-to-rim zonation in the complexes from the lowermost Kliening Complex toward the Micaschist Complex in the hanging wall [27,29]. P-T paths of metamorphism 1 and garnet 1 (M1, Grt1) in violet are related to Permian ages, P-T paths of metamorphism 2 and garnet 2 (M2, Grt2) in green are related to Cretaceous ages. Aluminosilicates (and Ky, Sil), cordierite-in (Cd+), muscovite-out (Ms-) and staurolite-in and -out (Sta+, Sta-) univariant lines [30]. Stability fields (green and gray) of monazite (Mnz) and allanite (Aln) at different bulk rock contents as a function of Ca wt%, and with the xenotime (Xtm) stability field. Bold cross was uncertainty of ± 50 °C/ ± 1.0 kbar on P-T estimates. Geothermobarometric data from eclogite marked in green box [71]. (e–h) Grossular-pyropo-spessartine (Grs-Prp-Sps) ternary diagrams of garnet core-to-rim (c, r) zonation, related to P-T paths in (a–d). (i–l) Histograms of monazite ages. Lack of Permian monazite ages in the lowermost Kliening Complex where no pegmatites were observed, contrasting Permian monazite populations in the other three complexes with pegmatites.

EPMA Th-U-Pb monazite ages have already been reported from the Kliening, Preims and Eclogite complexes [27,29], but not yet from the Micaschist Complex. For completion, monazite data from garnet micaschists, partly with staurolite, kyanite and chloritoid, are presented here (Table S1: Electron Probe Microanalyses of monazite in the Micaschist Complex of the Austroalpine Saualpe Nappes, Carinthia, Austria). Samples from the

structurally lower part of the Micaschist Complex displayed a mostly Permian monazite which defined ThO_2^* -PbO isochrons at 268 ± 34 Ma, 259 ± 9 Ma, 252 ± 16 Ma and 244 ± 7 Ma, partly accompanied by minor Carboniferous and Mesozoic populations (Figure 7a–c,f). Two samples displayed dominant Cretaceous monazites at isochrons of 87 ± 12 Ma and 87 ± 15 Ma (Figure 7d,e). The microstructural appearance of monazite in the Micaschist Complex was similar as already described from the underlying nappe units [27,29]. Of special interest were the various modifications of the monazite corona structures (Figure 2b–e). Such coronas of apatite end epidote around Permian monazite document a post-Permian retrograde metamorphic period [26,48]. Monazite corona structures were enclosed in second generation garnet with low Mn contents, indicating a prograde metamorphism subsequent to the retrogression period (Figure 2d,e).

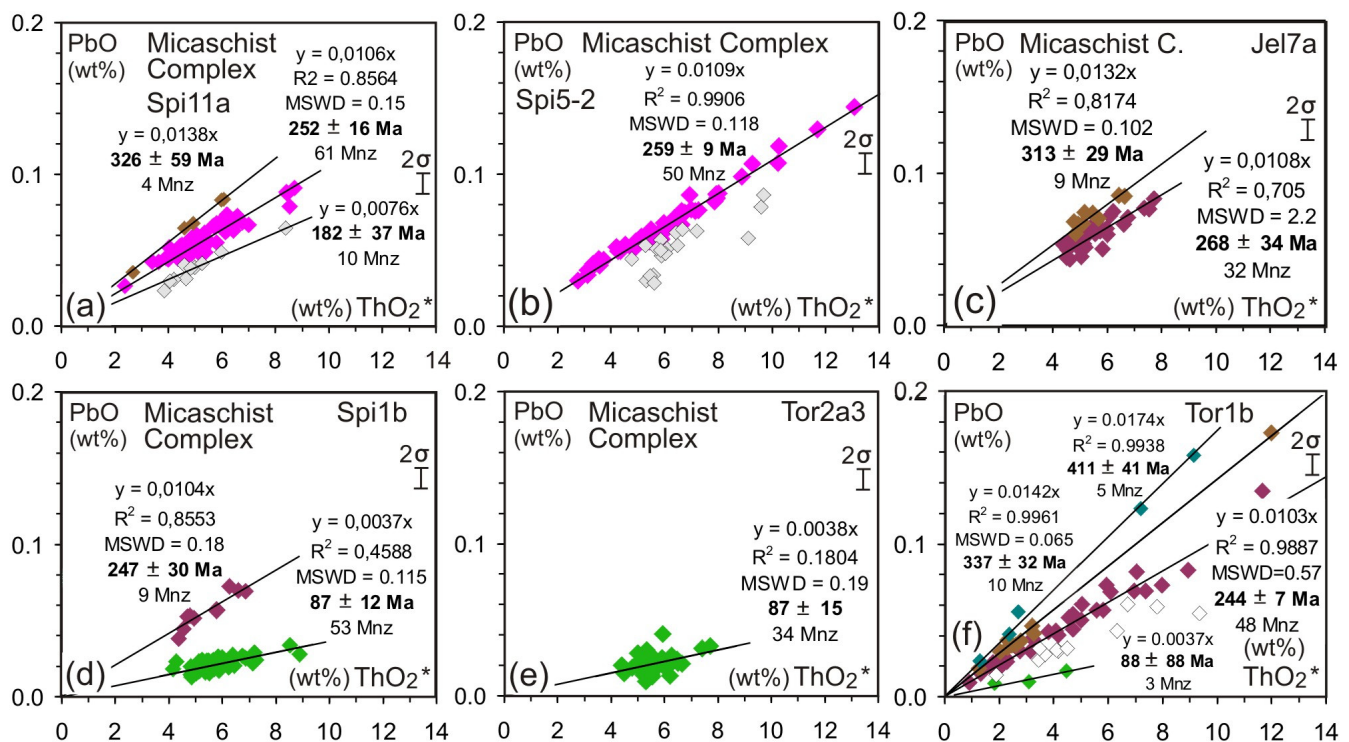


Figure 7. (a–f) Th-U-Pb chemical model ages of monazite in the Micaschist Complex of the Saualpe nappe stack. Total ThO_2^* -PbO (wt%) isochrone diagrams. ThO_2^* is $\text{ThO}_2 + \text{UO}_2$ equivalents expressed as ThO_2 . General minimal 2σ error on monazite PbO analysis is shown by a bar. Regression lines of monazite populations marked by colours give a coefficient of determination R^2 and were forced through zero. The coloured symbols mark analyses belonging to monazite age populations and defining isochrones, falling into Silurian (bluegreen), Carboniferous (brown), Permian (violet) and Cretaceous (green) ranges of ages; further Mesozoic monazite data are in white.

It was also interesting to compare the proportions of monazite age populations in the sample suites from the Saualpe nappe units (Figures 6i–l and 8). All samples had Al-rich and Ca-poor bulk rock compositions within narrow limits [27,29]. In the Kliening Complex, the samples were clearly dominated by Cretaceous monazite. Pre-Cretaceous monazites were lacking, although garnet one crystallisation was observed, as in the other complexes. In the Preims Complex, the Permian and Triassic monazites dominated and the Cretaceous monazites were quite scarce in some samples. In the Eclogite Complex, in most samples, the Permian monazites dominated, but three samples showed large populations of Cretaceous monazite. A similar situation was found in the Micaschist Complex where five samples were dominated by Permian and Triassic monazites and two samples mostly had Cretaceous monazites. Permian-Triassic monazite occurred only in the three complexes which showed pegmatite gneisses. This completes the observations

from the BSTW where Permian monazite was restricted to zones with Permian pegmatites. Apparently, the fluid-driven intrusion of the pegmatites induced a pervasive monazite crystallisation [27,29,62].

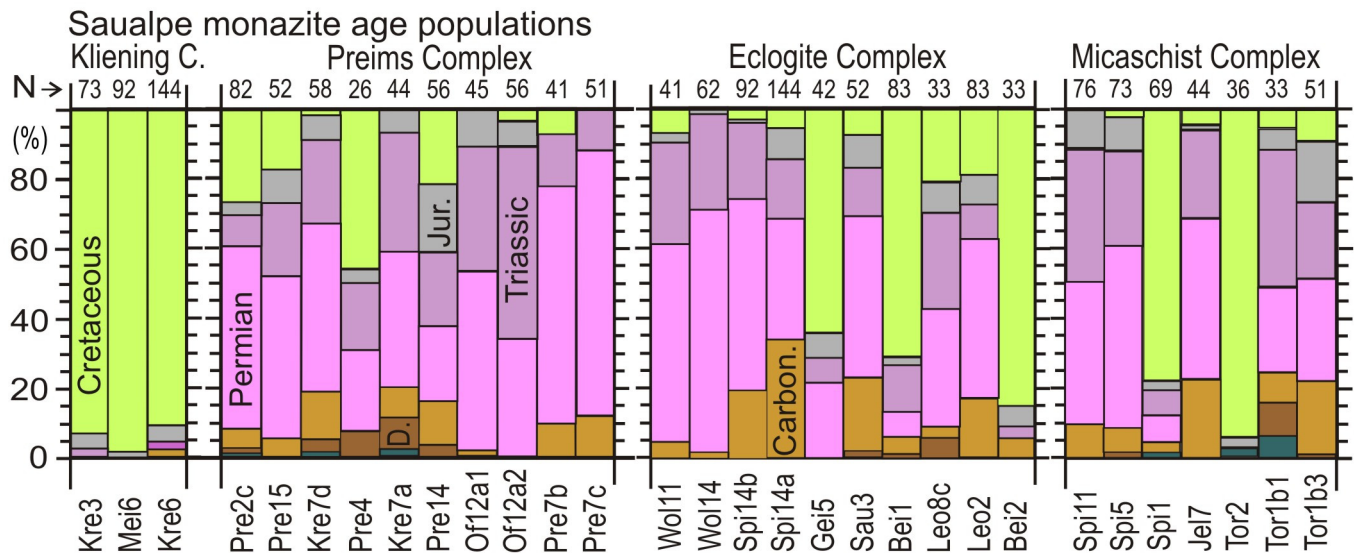


Figure 8. Kliening, Preims, Eclogite and Micaschist complexes in the Saualpe with diverse distribution of Silurian (blue-green), Devonian (D.), Carboniferous (Carb.), Permian, Triassic, Jurassic (Jur. in grey) and Cretaceous (140–60 Ma, in green) monazite ages recalculated to %, in single samples, partly compiled from data in [27,29].

4. Discussion

Garnet-bearing meta-psammopelites allowed reconstructions of P-T path segments in several Alpine basement terrains with geothermobarometry by cation exchange and net transfer continuous reactions. Syndeformational garnet-bearing assemblages crystallised during the formation of the main foliation. They recorded prograde metamorphism at an increasing pressure and temperature, followed by decreasing pressure with a further temperature increase. The maximum temperatures were mostly reached during the decompression. This corresponded to the standard clockwise P-T path in continental collision scenarios with tectonic crustal thickening, as demonstrated in classical numerical models [74,75]. It can also be shown by detailed garnet zonation studies that in several parts of the Alpine basement a second clockwise metamorphic cycle overprinted rocks which had undergone an earlier metamorphic cycle with higher (Aiguilles Rouges Massif) and also lower (BSTW, Saualpe) maximal thermal conditions (Figures 3a, 4a, 5a–d, 6a–d and 9a,d). The EPMA Th-U-Pb monazite dating revealed Ordovician-to-Silurian, Carboniferous, Permian and Cretaceous age populations. These major age populations are occasionally connected by minor Triassic and Jurassic populations (Figures 3g, 4g, 5i,l and 6i–l). The principal question is, how are these P-T path segments related to monazite crystallisation and ages, or which monazite generation may be linked to specific P-T path segments? Potential methods for performing such correlations to garnet are the monazite microstructures [48], monazite inclusions in garnet, monazite mineral chemistry [76], the stability fields of monazite and allanite [77–79] in reference to P-T path segments, and a combination of these.

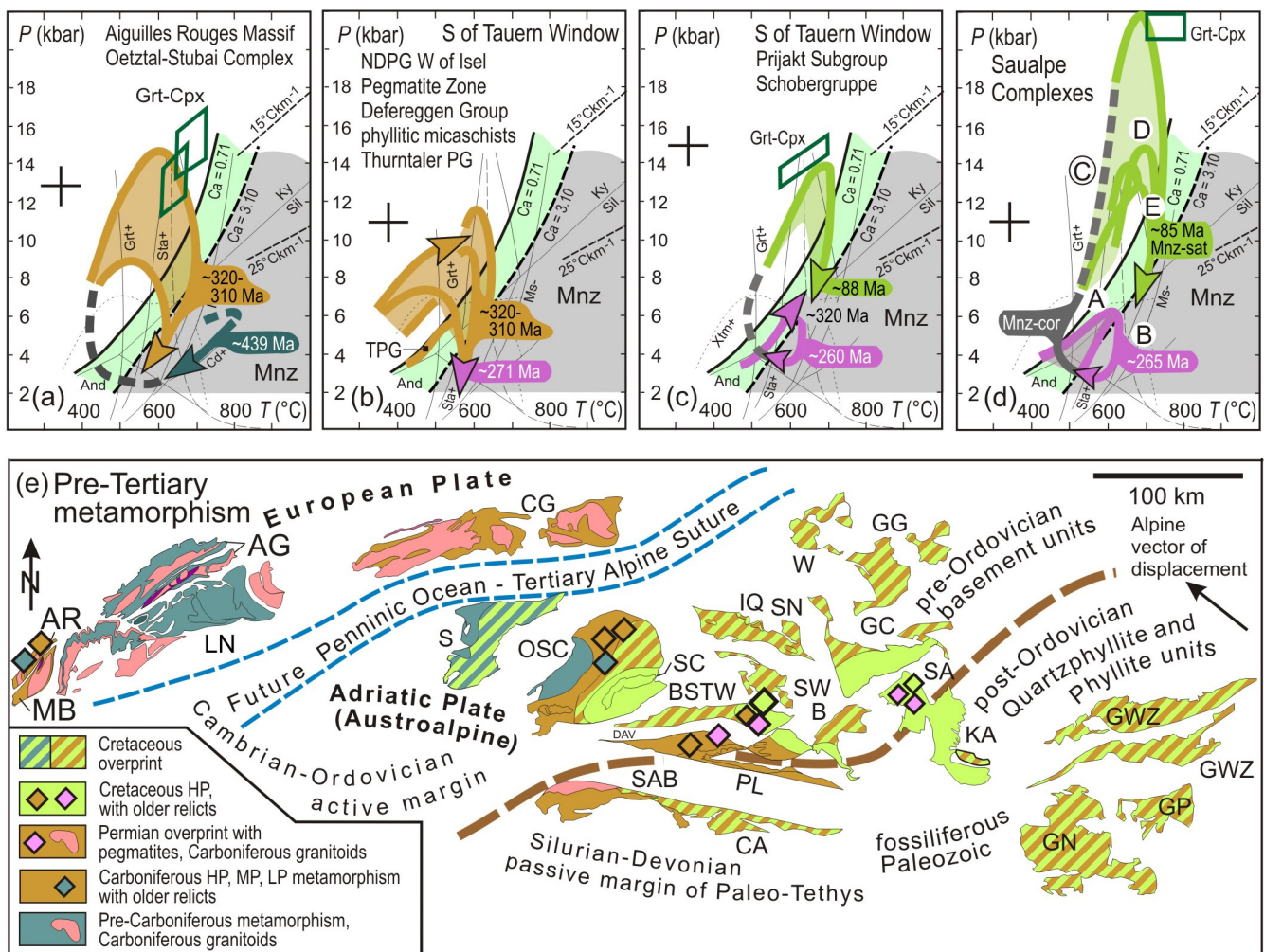


Figure 9. (a–d) Compilation and interpretation of P–T–time path segments in Alpine basement units from Figures 3–6. Aluminosilicates (And, Ky, Sill), cordierite-in (Cd+), muscovite-out (Ms-) and staurolite-in and -out (Sta+, Sta-) univariant lines [30]. Stability fields (green and gray) of monazite (Mnz) and allanite (Aln) at different bulk rock contents as a function of Ca wt%, and with the xenotime (Xtm) stability field [77,78]. P–T data (Grt–Cpx) from eclogites is given in green boxes. Bold cross is uncertainty of $\pm 50^\circ\text{C}/\pm 1.0\text{ kbar}$ on P–T estimates. Distinct parts of the P–T path segments are labelled with Ordovician-to-Silurian (dark green), Carboniferous (brown), Permian (purple) and Cretaceous (light green) monazite ages in Ma. For labelling A–E of P–T path segments in Saualpe complexes (d) see text. (e) Selected Alpine basement units in a pre-Mesozoic configuration, following mainly a palinspastic restoration. The main Tertiary Alpine displacement vector of basement units is SE–NW. Basement units belong to a Cambrian–Ordovician active margin and a Silurian–Devonian passive margin setting [3]. The assignment of basement units to pre-Tertiary metamorphic periods follows the map of metamorphism in the Alps [2]. Locations reported here are marked with colors of monazite age populations. Abbreviations of basement units and major tectonic lines: AG Aar–Gotthard; AR Aiguilles Rouges; B Bundschuh; BSTW Basement to the south of Tauern Window; CA Carnic Alps; CG Central Gneisses; DAV Defereggeng–Antholz–Vals Line; GC Gleinalm Complex; GG Grobgneis Complex; GN Gurktal nappes; GP Palaeozoic of Graz; GWZ Greywacke Zone; IQ Innsbruck Quartzphyllite; KA Koralpe; LN Leontine Nappes; MB Mont Blanc; OSC Oetztal–Stubai Complex; PL Periadriatic Lineament; S Silvretta; SA Saualpe; SAB South Alpine Basement; SC Schneeberg Complex; SP Speik Complex with Kraubath ophiolite; TPG Thurntaler Phyllite Group; TW Tauern Window; W Wechsel Gneiss Complex.

In mylonitic garnet gneisses in the Aiguilles Rouges Massif, the pyrope-rich garnet cores crystallised at 6 kbar/800 °C. This was inside the monazite stability field, even for more Ca-rich bulk rock compositions (Figure 3a,b). Ordovician-to-Silurian monazites are abundant and prevail in these samples (Figure 3e). The Carboniferous monazites in the samples occurred often in satellite structures (Figure 2f,g), which implies a prograde

metamorphism subsequent to a retrogressive event [80]. Furthermore, the Carboniferous monazites in the mylonitic garnet gneisses occurred within fine-grained high temperature mylonitic layers which surround microlithons with the large garnet porphyroblasts. This allowed to relate the crystallisation of the garnet to an Ordovician-to-Silurian monazite crystallisation event [47]. The P-T paths reconstructed from the strongly zoned garnets in micaschist samples entered the monazite stability field at heating-decompression (Figure 3a,c,d). In these samples, the Carboniferous monazites prevailed and indicated the age of crystallisation of the pyrope-rich garnet rims. P-T conditions retrieved from the amphibolitised eclogites apparently matched the initial stage of the P-T path for the micaschists to the W, signalling also a Carboniferous metamorphism (Figure 9a). However, this should be confirmed by independent Sm-Nd or Lu-Hf dating of the metabasite garnet.

In the northern part of the Oetztal-Stubai Complex, outside the zone with Cretaceous biotite K-Ar ages, but partly within the Cretaceous chloritoid zone, the Carboniferous monazite ages clearly prevailed (Figure 4e–g). Ordovician-to-Silurian monazite ages were restricted to distinct locations such as the Winnebach and other migmatites, but occurred also in single grains sporadically in some micaschist samples [53,58]. P-T path segments of a prograde metamorphism with maximal pressures at 13 kbar/600 °C were followed by decompression-heating to maximal 6 kbar/680 °C, and further decompression-cooling. The pre-P_{max} evolution was outside the monazite stability field, even for low Ca bulk rock compositions. P-T paths of decompression-heating also entered the monazite stability field for more Ca-rich bulk rock compositions, as for the Stubai samples (Figure 4a–d). As a consequence, the maximum of the Carboniferous monazite age distribution at 321 ± 2 Ma could be related to the maximal temperature approached during a Carboniferous metamorphic cycle. This would match with a 360–350 Ma Sm-Nd age of eclogite garnets, interpreted to date the high pressure stage [50]. It can be concluded that the Carboniferous monazites started to crystallise during decompression after the pressure maximum when the P-T path enter the monazite stability field for the given Ca bulk rock compositions. A continuing crystallisation of successively younger monazites, often in cluster microstructures, occurred during further decreasing pressures within the stability field of sillimanite. Conditions for monazite crystallisation even for elevated bulk rock Ca compositions maintained when the P-T path passed into the andalusite stability field and may have led to some Permian monazites [41]. The Cretaceous metamorphic overprint in this part of the OSC, apparently, occurred at P-T conditions outside the monazite stability field and appeared as a retrogressive event, which was documented by double corona allanite-apatite structures around the relic Carboniferous monazite [41,53,58].

In the Defereggeng Group of the Austroalpine basement to the south of the Tauern Window, the Carboniferous monazite ages prevailed. Thermobarometry revealed prograde P-T path sections with maximal pressures at about 10 kbar/600 °C, followed by decompression (Figure 5a,e). As in the OSC, this allowed to conclude to a Carboniferous high pressure amphibolite facies metamorphism along clockwise P-T paths [16,61]. However, in the Defereggeng Group, no amphibolitised eclogites as in the OSC or AR were observed. In the hanging wall of the Defereggeng Group, the maximal pressures in phyllitic micaschists were at 7 kbar. In the Steinkogel Nappe with similar garnet zonations in the micaschists, only slightly higher pressures at 9 kbar/520 °C were attained (Figure 5b,f and Figure 9b). In the Thurntaler Phyllite Group, the maximal pressures were even lower, at 5–6 kbar. The age of this metamorphism at a medium pressure was also Carboniferous, as could be concluded from the mica cooling ages in these parts of the basement [16,60]. When compared to the P-T and monazite age data from the OSC, one can state that there was a trend of decreasing maximal pressures within the units with Carboniferous metamorphism, and also a trend toward younger, but still Carboniferous, monazite ages within the Austroalpine basement units. Permian pegmatites occurred at the base of the Defereggeng Group in a distinct zone to the south, and also to the north of the DAV in the North-Defereggeng-Petzeck Group. Maximal pressures of 10–12 kbar/600 °C could be retrieved by thermobarometry of micaschist host rocks. In some of the samples, the garnet zonations displayed a decrease in the

grossular toward the rims, resulting in marked decompression paths, partly approaching 4 kbar/580 °C (Figure 5c,g). Permian monazite ages prevailed, as observed from other zones with Permian pegmatites (Figure 5j,k). Garnet zonations in micaschists, P-T data and P-T path segments were similar to those observed in the OSC and in the Defereggeng Group, and the monazite stability field was approached also during the decompression paths. The difference was that Permian and not Carboniferous monazites prevailed in this zone. It has been claimed that the Permian pegmatites crystallised at low pressures, as they occurred with andalusite [23]. Additionally, when the Permian pegmatites were not foliated and transposed to gneisses, they cut across an older foliation [16]. Upon combining these observations, it appeared as possible that the Permian pegmatites intruded during the uplift of the crust subsequent to the Carboniferous metamorphism, or in terms of P-T paths, when the decompression paths approached low pressure conditions subsequent to the Carboniferous medium pressure stages (Figure 9b). As the conditions of pegmatite crystallisation were within the monazite stability field, and as these intrusions were accompanied by fluids, this may have enhanced a pervasive monazite crystallisation in the host rocks.

In the Prijakt Subgroup in the Schobergruppe, a trimodal distribution of monazite age populations was observed [62]. Carboniferous monazites were dominant in some micaschist samples, whereas Permian monazites were abundant in samples next to pegmatites. Inclusions of Permian monazites in the garnet with low spessartine contents, and clustered crystallisation of tiny Cretaceous monazite (Figure 2i) in a sample HPr10 with low spessartine and high grossular contents in the garnet allowed the conclusion that a garnet two generation belongs to a Cretaceous high pressure metamorphism [62]. This confirms the Cretaceous Lu-Hf garnet ages in amphibolitised eclogites [66]. The zonations of the garnet one porphyroblasts in the Prijakt Subgroup differed considerably from those in the other parts of the BSTW. They displayed low grossular contents and, significantly, increasing pyrope contents toward the rims (Figure 5e–h). The accordingly calculated prograde P-T path segments started at low pressures and approached 6 kbar/600 °C which was the monazite stability field for low Ca bulk rock compositions (Figures 5d and 9c). According to the structural observations, this prograde P-T path segment should have predated the pegmatite intrusions, presumably at late Carboniferous or early Permian times.

The evolution of the micaschists in the Saualpe complexes was characterised by the crystallisation of garnet one and garnet two at the M1 and M2 metamorphic events, and two monazite generations at Permian and Cretaceous times. For the correlation of garnet and monazite generations, the metamorphic evolution in the Saualpe complexes was subdivided into five stages, A to E [27,29]. Stages A and D correspond to the garnet one and garnet two crystallisation at the M1 and M2 events. The Permian monazites represent the stage B and the Cretaceous monazites the stage E. Stage C corresponds to the time gap between the M1 and M2 metamorphic events and the Permian and Cretaceous monazites (Figure 6c).

The garnet one assemblages in the Saualpe complexes uniformly recorded a first prograde metamorphism M1 (stage A) along an intermediate P-T gradient toward maximal pressures of 6 kbars at temperatures ranging between 600 and 650 °C (Figure 6a–d). For event M2, with garnet two assemblages (stage D), the maximal conditions were different and matched the occurrence and absence of eclogites [27,29,68,70,71]. Except for the Kliening Complex where Permian monazites as well as pegmatites were lacking, the other complexes displayed bimodal distributions of Permian and Cretaceous monazite ages, despite the diverse age distributions in single samples (Figure 6e–h, Figures 7 and 8). Monazite Y_2O_3 and HREE contents potentially increased with a metamorphic grade [76]. Most of the bulk rock Y and HREE would be fractionated into garnet one and into the oldest monazites, the Permian populations. This will reduce the availability for Y and HREE, especially Gd, for the crystallisation of garnet two and the later Cretaceous monazite. Therefore, a Y saturation in the Cretaceous monazite is not necessarily the case. The

observed lower Y and Gd in Cretaceous monazites compared to the Permian monazites, then, would not indicate lower formation temperatures. Maximal temperatures during M2 exceeded those at M1 in all Saualpe complexes [27,29]. As a consequence, the Y-rich Permian monazite should date the metamorphism M1 with garnet one at lower temperatures, and not the M2 event where garnet two crystallised at higher temperatures.

The apatite-allanite corona structures around Permian monazite in the allochthonous Saualpe complexes (Figure 2e,f) were interpreted as an indicator for monazite decomposition. A fluid-mediated coupled dissolution-precipitation process can explain the pseudomorphic partial replacement of the original monazite by apatite and allanite [26,81]. Such monazite corona structures were generated during a decreasing temperature at retrogression [81]. In several samples, a Permian monazite with a corona structure was enclosed by a garnet two porphyroblast (Figure 2e,f). The most likely interpretation of this observations would be a post-Permian and post-monazite-corona crystallisation of garnet two. Furthermore, garnet one recorded a prograde metamorphism M1. It appears unlikely that garnet one crystallised at the same time when Permian monazite underwent retrogression; it should have crystallised previous to the retrogression event. This signals an early Permian minimum age of garnet one. A general assumption is that the garnet should be younger than the enclosed monazite. This may be true when the monazite is significantly older than the bulk of the matrix monazite. In contrast, monazite may crystallise after garnet formation along cracks or pits of the host mineral. Monazite could then be younger or of the same age as the hosting garnet [48]. In many samples, Permian monazites were enclosed in spessartine-poor garnet two porphyroblasts, signalling their post-Permian crystallisation [27,29]. The microstructure of satellite monazite with Cretaceous ages was occasionally observed in the pegmatite-bearing complexes of the Saualpe. These monazite satellite grains should have crystallised during an increase in temperature after the formation of allanite-apatite coronas surrounding the monazite [80]. Monazite microstructures, thus, can confirm that there was a period of decreasing and then increasing P-T conditions which separated the two prograde metamorphic events.

The prograde P-T path for the garnet one assemblage in the Saualpe complexes matched the monazite stability field only for low Ca bulk compositions (Figures 6a–d and 9d). Monazite crystallisation started when the prograde P-T path of M1 entered the monazite stability field at a high temperature, or, subsequently, at a decreasing pressure for the relevant bulk composition. This also suggests an early Permian minimum age for the garnet one assemblage. Favourable P-T conditions for extensive Permian-to-Triassic (290–200 Ma) monazite crystallisation (labelled as stage B) can be expected during decreasing pressure, subsequent to the garnet one growth. It has been suggested from thermodynamic modelling of garnet-bearing assemblages with and without staurolite, that garnet should not crystallise and may be consumed or resorbed during the isothermal decompression and decompression accompanied by cooling [30,79]. Partial resorption and consumption of the garnet result in gaps, breaks and marked discontinuities in the P-T record. The crystallisation of the Permian monazite subsequent to garnet one was further supported by the pervasive intrusion of Permian to Triassic pegmatites. Such intrusions into metamorphic host rocks were initiated by fluids, which would facilitate monazite crystallisation. Studies of Permian to Triassic pegmatites in the Eastern Alps [22,72,82] claim a contemporaneous low-pressure metamorphism with andalusite and sillimanite formation during their emplacement. As for a decompression and cooling evolution, such a low pressure event would not be favourable for garnet crystallisation. If garnet growth is not favoured, the pegmatite intrusions should postdate the peak pressure conditions recorded by garnet one with an early Permian minimum age. As a consequence, the garnet one assemblage should belong to a metamorphism at an intermediate P-T regime previous to a Permian to Triassic low pressure high temperature event accompanied by pervasive pegmatite intrusions.

For the corona formation of Permian monazite (stage C) of the metamorphic evolution (Figure 9d), the low temperature stability limit of monazite should have been passed

during a decrease in temperature and/or at a re-increase in pressure, when the high P-T conditions of garnet two crystallisation were achieved. The P-T conditions for garnet two crystallisation (stage D) in the Saualpe complexes were not favourable for extensive monazite formation as they were apparently outside the monazite stability field (Figure 9d). An age assessment of the high pressure garnet two crystallisation was facilitated by the comparably narrow time span of the Cretaceous monazites around 95–81 Ma [27,29]. It was suggested that these monazites crystallised after garnet two when, at further decompression, P-T conditions more favourable to the monazite stability field were achieved. This was labelled as stage E of the evolution (Figure 9d). In general, these Cretaceous monazite ages coincide with Sm-Nd data from the eclogites at 95–88 Ma, [70,71]. The Ar-Ar mica ages at 86–78 Ma [67] were slightly younger, as can be expected, and date cooling after peak P-T conditions. The EPMA monazite ages can, thus, confirm the known range of age data for the Cretaceous high pressure event and the subsequent cooling.

For the Carboniferous-to-Permian metamorphism during the Variscan orogeny, the monazite ages and thermobarometric data signalled two separate thermal and spatial events. On the one hand, clockwise P-T path segments were observed which started at low a temperature and medium-to-high pressure in the kyanite stability field far outside the monazite stability field. These P-T paths passed eclogite facies conditions in the Aiguilles Rouges Massif and the Oetztal-Stubai Complex, and high pressure amphibolite facies conditions in the BSTW. Carboniferous monazite ages at ~320–310 Ma can be related to the decompression-heating and decompression-cooling P-T path sections. There were units with lower maximal pressures (~10–8 kbar), but also prograde P-T paths within in the kyanite stability field. Although monazite ages were partly not available from these units, one can conclude to a Carboniferous metamorphism due to corresponding mica cooling ages. Furthermore, the units with such Carboniferous metamorphism had pre-Early Ordovician sedimentary deposition ages and orthogneisses, the former Ordovician granitoids, in common. In the Thurntaler Phyllite Group with a post-Early Ordovician sedimentation age [13,16], the pre-Alpine metamorphism started at low pressures and the maximal pressures remained below 6 kbar, contrasting the more pressure-dominated Carboniferous P-T path segments in the other units. A special situation with marked decompression paths was observed in the pegmatite bearing basement parts to the north and the south of the Deferegggen-Antholz-Vals Line. There, it appeared likely that the Permian pegmatites intruded at low pressures subsequent to the pre-Alpine decompression path segments. To sum up, the pressure-dominated Carboniferous metamorphism along clockwise P-T paths displayed maximal pressures ranging between the geothermal gradients of 15 °C/km and 25 °C/km.

In the basement areas with a Cretaceous high-pressure metamorphism, as the Prijakt Subgroup and the Saualpe, one observes a garnet one generation with zonations along low grossular contents which contrasted the zonations in the units with Carboniferous monazite. The geothermobarometry of the garnet-bearing assemblages gave prograde P-T path segments which started at low pressures, reach maximal pressures at around 6 kbar/600 °C and rarely showed final decompression. In the Saualpe, these contrasting P-T evolutions could be categorised as early Permian due to the dominant Permian monazite ages. In the Prijakt Subgroup of the BSTW, with a similar P-T path, this age classification was not free of doubt, as a distinct population of Carboniferous monazite exists there. However, a Permian metamorphism at an intermediate P-T regime has been reported from regions adjacent to the Saualpe [82–84]. It should have preceded a Permo-Triassic low pressure stage with the intrusion of pegmatites.

For the Cretaceous metamorphism, one observes comparable garnet compositions and zonations, but different maximal pressures in the various basement regions. Apparently, in the Saualpe Eclogite Complex, the maximal pressures considerably exceeded those in the underlying and also overlying units. In the Prijakt Subgroup of the BSTW with amphibolitised eclogites, the maximal pressures were also lower as in the Saualpe Eclogite Complex. The geothermal gradients corresponding to the maximal pressures were at

15 °C/km and lower for the Cretaceous metamorphism. The Cretaceous monazite ages uniformly displayed unimodal distributions around ~85 Ma and were interpreted to date the decompression-cooling stage after the high pressure stage.

The polyphase metamorphism of the pre-Mesozoic basement units as deciphered by the P-T and monazite age data also had spatial aspects, as presented in a pre-Tertiary palinspastic reconstruction [85] in combination with the map of pre-Tertiary metamorphism [2]. Basement units with Ordovician-to-Silurian events and the high pressure Carboniferous metamorphism were situated to the NW (Figure 9e). Basement units with Carboniferous metamorphism at lower maximal pressures occurred in the central part, and units with the early Permian metamorphism as exemplified in the Saualpe complexes followed towards the SE. Monazite crystallisation and ages are apparently not only related to the decompression P-T paths of regional metamorphic events, but also to the intrusion of the Austroalpine Permian pegmatites. The pegmatite-bearing zone cuts across various Austroalpine units, with and without Ordovician granitoids (Figure 1). The Cretaceous metamorphism and overprint at different grades and maximal pressures was restricted to the Austroalpine basement. The maximal pressures of the Cretaceous metamorphism were observed not at the margins, but in the more central parts of the Austroalpine domain, namely, in the Saualpe, Koralpe and Pohorje complexes (Figure 9e).

5. Conclusions

The combined approach with EPMA Th-U-Pb monazite dating and microstructurally controlled geothermobarometry of garnet-bearing assemblages in metapelites allowed to reveal several pre-Tertiary metamorphic events in Alpine basement units. Monazite ages concentrated around Ordovician-to-Silurian (~450–420 Ma), Carboniferous (320–310 Ma), Permian (~265 Ma) and Cretaceous (~100–85 Ma) populations and isochrons. Single samples displayed unimodal, bimodal and rarely trimodal distributions of monazite age populations. The variable distributions of age populations implicated to combine data from several samples for a complete characterisation.

An interpretation of various P-T path sections reconstructed from zoned garnets in assemblages with biotite, muscovite, plagioclase, aluminosilicate(s) and quartz in reference to the monazite stability field and the microstructures allowed a temporal assignment of the metamorphic events. Accordingly, monazite crystallised posterior to the maximal pressures during the decompression-heating and decompression-cooling sections of each clockwise P-T evolution. Furthermore, the intrusion of pegmatites along a distinct zone in the Austroalpine domain was accompanied by the crystallisation of Permian monazite.

The earliest event of the polymetamorphic evolution in the Alpine basement was an Ordovician-to-Silurian (439 ± 14 Ma) metamorphism at 6 kbar/800 °C in the Aiguilles Rouges Massif, and a migmatization in distinct areas in the Oetztal-Stubai Complex. Due to the sparse complementary information, the geodynamic significance of this event remained spurious. It can be suggested that this temperature-dominated metamorphism was part of an Early Paleozoic arc magmatism.

A subsequent pressure-dominated metamorphism can be assigned to Carboniferous (320–310 Ma) monazite crystallisation in the course of the decompression-heating and decompression-cooling P-T path sections. This Carboniferous metamorphism along clockwise P-T paths signalled a continental collision with crustal thickening. The Carboniferous metamorphism displayed different maximal pressures, in the various basement units, ranging between 16 and 6 kbars, and with eclogite facies conditions in units to the NW. In basement units to the SE, especially in the Saualpe nappe complex, a distinct initial early Permian metamorphism at maximal 6 kbar/600–650 °C of which P-T path segments started at a low pressure (~4 kbar/500 °C) preceded the intrusion of the Permian pegmatites. This scenario can be explained by the extension of a moderately thickened crust subsequent to a continental collision.

The Austroalpine basement units to the SE were overprinted by a Cretaceous high pressure metamorphism with P-T path segments along overall clockwise P-T paths. Monazite

with ages at around ~85 Ma dates the decompression stage. The Cretaceous metamorphism can be related again to a continental collision scenario with crustal thickening, but at a higher P-T and lower geothermal gradients when compared to the Carboniferous and Permian events. The Tertiary (Late Alpine) metamorphism since the Eocene was prominent in many basement units of the Alps. A critical point of the EPMA Th-U-Pb monazite dating method was the limit of detection for Pb. The amount of radiogenic Pb in monazite generated from the decay of Th and U since the Tertiary was mostly too low to be reliably measured by EPMA. However, in the studied units no monazite with low Pb contents corresponding to Tertiary ages was detected.

The pre-Tertiary polymetamorphism in the various Alpine basement units was obvious by the crystallisation of garnet porphyroblast generations with different endmember compositions and zonations. Early metamorphic events were followed by decompression and cooling toward P-T conditions outside the monazite stability field. This led to the corona microstructures of monazite decomposition, signalling a retrogression. The re-increase in temperature and pressure during the second and later metamorphic overprint led to the re-crystallisation of considerably younger monazite in satellite microstructures.

Supplementary Materials: The following are available online at <https://www.mdpi.com/article/10.3390/min11090981/s1>, Table S1: Electron Probe Microanalyses of monazite in the Micaschist Complex of the Austroalpine Saualpe Nappes (Carinthia, Austria).

Funding: The Deutsche Forschungsgemeinschaft (DFG) supported numerous field studies on monazite Th-U-Pb dating in the Alps by grants (SCHU-676/10, 676-11, 676-12, 676-13, 676-15, 676-20). The Open Access and APC was financed by the Publication Fund of the TU Bergakademie Freiberg.

Data Availability Statement: Tables of EPMA Th-U-Pb monazite and silicate minerals measurements related as Supplementary Materials to the referenced publications can be obtained by request from the author.

Acknowledgments: The author appreciates the initiation and permanent motivation for monazite studies through Fritz Finger from Salzburg. Monazite dating by electron probe microanalyser required long-term analytical sessions which were facilitated at the Geozentrum Nordbayern of Universität Erlangen-Nürnberg, Institute of Materials Sciences at TU Bergakademie Freiberg/Saxony and with Joachim Krause at Helmholtz Institute Freiberg for Resource Technology. Support at the SEM studies in the Laboratory of Geometallurgy at TU Bergakademie Freiberg was accomplished by Sabine Gilbricht. The author also acknowledges the constructive contributions of the three reviewers to the manuscript.

Conflicts of Interest: The author declares no conflict of interest.

References

1. Schmid, S.M.; Fügenschuh, B.; Kissling, E.; Schuster, R. Tectonic map and overall architecture of the Alpine orogen. *Swiss J. Geosci.* **2004**, *97*, 93–117. [[CrossRef](#)]
2. Frey, M.; Desmons, J.; Neubauer, F. The new metamorphic map of the Alps: Introduction. *Swiss Bull. Mineral. Petrol* **1999**, *79*, 1–4. [[CrossRef](#)]
3. Von Raumer, J.F.; Neubauer, F. *The Pre-Mesozoic Geology in the Alps*; Springer: Berlin/Heidelberg, Germany, 1993; p. 677.
4. Von Raumer, J.F.; Bussy, F.; Schaltegger, U.; Schulz, B.; Stampfli, G.M. Pre-Mesozoic Alpine basements—Their place in the European Paleozoic framework. *GSA Bull.* **2012**, *125*, 89–108. [[CrossRef](#)]
5. Spear, F.S.; Selverstone, J. Quantitative P-T paths from zoned minerals: Theory and tectonic applications. *Contrib. Miner. Pet.* **1983**, *83*, 348–357. [[CrossRef](#)]
6. Jäger, E. Rb-Sr Systems in different degrees of metamorphism. *Eclogae Geol. Helv* **1970**, *63*, 163–172. [[CrossRef](#)]
7. Thöni, M. Degree of evolution of the Alpine metamorphism in the Austroalpine unit W of the Hohe Tauern in the light of K/Ar and Rb/Sr age determinations on micas. *Jahrb. Geol. Bundesanst.* **1981**, *124*, 111–174.
8. Frank, W.; Kralik, M.; Scharbert, S.; Thöni, M. Geochronological data from the Eastern Alps. In *Geodynamics of the Eastern Alps*; Flügel, H.W., Faupl, P., Eds.; Franz Deuticke: Wien, Deuticke, 1987; pp. 272–281.
9. Montel, J.-M.; Foret, S.; Veschambre, M.; Nicollet, C.; Provost, A. A fast, reliable, inexpensive in-situ dating technique: Electron microprobe ages on monazite. *Chem. Geol.* **1996**, *131*, 37–53. [[CrossRef](#)]
10. Suzuki, K.; Kato, T. CHIME dating of monazite, xenotime, zircon and polycrase: Protocol, pitfalls and chemical criterion of possibly discordant age data. *Gondwana Res.* **2008**, *14*, 569–586. [[CrossRef](#)]

11. Williams, M.L.; Jercinovic, M.J.; Mahan, K.H.; Dumond, G.; Kohn, M.J.; Engi, M.; Lanari, P. 5. Electron Microprobe Petrochronology. *Petrochronology* **2017**, *83*, 153–182. [[CrossRef](#)]
12. Spear, F.S.; Pyle, J.M. Apatite, Monazite, and Xenotime in Metamorphic Rocks. *Rev. Miner. Geochem.* **2002**, *48*, 293–335. [[CrossRef](#)]
13. Siegesmund, S.; Oriolo, S.; Schulz, B.; Heinrichs, T.; Basei, M.A.S.; Lammerer, B. The birth of the Alps: Ediacaran to Paleozoic accretionary processes and crustal growth along the northern Gondwana margin. *Int. J. Earth Sci.* **2021**, *110*, 1321–1348. [[CrossRef](#)]
14. Frisch, W.; Neubauer, F. Pre-Alpine terranes and tectonic zoning in the eastern Alps. *Geol. Soc. Am. Spec. Pap.* **1989**, *230*, 91–100. [[CrossRef](#)]
15. Schaltegger, U.; Nægler, T.; Corfu, F.; Maggetti, M.; Galetti, G.; Stosch, H.G. A Cambrian island arc in the Silvretta nappe: Constraints from geochemistry and geochronology. *Swiss Bull. Mineral. Petrol.* **1997**, *77*, 337–350.
16. Schulz, B.; Steenken, A.; Siegesmund, S. Geodynamics of an Alpine terrane—the Austroalpine basement to the south of the Tauern Window as a part of the Adriatic Plate. In *Tectonic Aspects of the Alpine-Dinaride-Carpathian System*; Siegesmund, S., Fügenschuh, B., Froitzheim, N., Eds.; Tectonic aspects of the Alpine-Dinaride-Carpathian system. *Geol. Soc. Lond. Spec. Publ.* **2008**, *298*, 5–43.
17. Schaltegger, U.; Abrecht, J.; Corfu, F. The Ordovician orogeny in the Alpine basement: Constraints from geochronology and geochemistry in the Aar Massif (Central Alps). *Swiss Bull. Mineral. Petrol.* **2003**, *83*, 183–239. [[CrossRef](#)]
18. Franz, L.; Romer, R.L. Caledonian high-pressure metamorphism in the Strona-Ceneri Zone (Southern Alps of southern Switzerland and northern Italy). *Swiss J. Geosci.* **2007**, *100*, 457–467. [[CrossRef](#)]
19. Zurbriegen, R. The Cenerian orogeny (early Paleozoic) from the perspective of the Alpine region. *Int. J. Earth Sci.* **2017**, *106*, 517–529. [[CrossRef](#)]
20. Bousquet, R.; Schmid, S.; Zeilinger, G.; Oberhänsli, R.; Rosenberg, C.; Molli, G.; Robert, C.; Wiederkehr, M.; Rossi, P. *Tectonic Framework of the Alps (1:1,000,000)*; Commission for the Geological Map of the World: Reston, VA, USA, 2012.
21. Thöni, M. A review of geochronological data from the Eastern Alps. *Swiss Bull. Mineral. Petrol.* **1999**, *79*, 209–230.
22. Schuster, R.; Scharbert, S.; Abart, R.; Frank, W. Permo-Triassic extension and related HT/LP metamorphism in the Austroalpine–Southalpine realm. *Mitt. Ges. Geol. Bergbaustud. Österr.* **2001**, *45*, 111–141.
23. Schuster, R.; Ilickovic, T.; Mali, H.; Huet, B.; Schedl, A. Permian pegmatites and spodumene pegmatites in the Alps: Formation during regional scale high temperature/low pressure metamorphism. In *Proceedings of the 8th International Symposium on Granitic Pegmatites*, Kristiansand, Norway, 9–13 June 2017; pp. 122–125.
24. Habler, G.; Thöni, M. Preservation of Permo-Triassic low-pressure assemblages in the Cretaceous high-pressure metamorphic Saualpe crystalline basement (Eastern Alps, Austria). *J. Metamorph. Geol.* **2001**, *19*, 679–697. [[CrossRef](#)]
25. Mair, V.; Nocker, C.; Tropper, P. Das Ortler-Campo Kristallin in Südtirol. *Mitt. Österr. Mineral. Ges.* **2007**, *153*, 219–240.
26. Hentschel, F.; Janots, E.; Trepmann, C.A.; Magnin, V.; Lanari, P. Corona formation around monazite and xenotime during greenschist-facies metamorphism and deformation. *Eur. J. Mineral.* **2020**, *32*, 521–544. [[CrossRef](#)]
27. Schulz, B.; Krause, J. Electron probe petrochronology of polymetamorphic garnet micaschists in the lower nappe units of the Austroalpine Saualpe basement (Carinthia, Austria). *Z. Dtsch. Ges. Geowiss.* **2021**, *172*, 19–46. [[CrossRef](#)]
28. Schulz, B.; Sandmann, D.; Gilbricht, S. SEM-based Automated Mineralogy and its Application in Geo- and Material Sciences. *Minerals* **2020**, *10*, 1004. [[CrossRef](#)]
29. Schulz, B. Polymetamorphism in garnet micaschists of the Saualpe Eclogite Unit (Eastern Alps, Austria), resolved by automated SEM methods and EMP-Th-U-Pb monazite dating. *J. Metamorph. Geol.* **2016**, *35*, 141–163. [[CrossRef](#)]
30. Spear, F.S. Metamorphic Phase Equilibria and Pressure-Temperature-Time Paths. In *Mineralogical Society of America Monograph Series*; Mineralogical Society of America: Washington, DC, USA, 1993; Volume 1, p. 799.
31. Powell, R.; Holland, T.J.B. On thermobarometry. *J. Metamorph. Geol.* **2008**, *26*, 155–179. [[CrossRef](#)]
32. Holland, T.J.B.; Powell, R. An improved and extended internally consistent thermodynamic dataset for phases of petrological interest, involving a new equation of state for solids. *J. Metamorph. Geol.* **2011**, *29*, 333–383. [[CrossRef](#)]
33. Schulz, B. P-T-deformation paths of Variscan metamorphism in the Austroalpine basement: Controls on geothermobarometry from microstructures in progressively deformed metapelites. *Swiss Bull. Mineral. Petrol.* **1993**, *73*, 274. [[CrossRef](#)]
34. Schulz, B.; Triboulet, C.; Audren, C.; Feybesse, J.-L. PT-paths from metapelite garnet zonations, and crustal stacking in the Variscan inverted metamorphic sequence of La Sioule, French Massif Centra. *Z. Dtsch. Geol. Ges.* **2001**, *152*, 1–25.
35. Passchier, C.W.; Trouw, R.A.J. *Microtectonics*, 2nd ed.; Springer: Berlin/Heidelberg, Germany, 2005; p. 289.
36. Wu, C.-M. Revised empirical garnet-biotite-muscovite-plagioclase geobarometer in metapelites. *J. Metamorph. Geol.* **2014**, *33*, 167–176. [[CrossRef](#)]
37. Pyle, J.M.; Spear, F.S.; Wark, D.A.; Daniel, C.G.; Storm, L.C. Contributions to precision and accuracy of monazite microprobe ages. *Am. Miner.* **2005**, *90*, 547–577. [[CrossRef](#)]
38. Jercinovic, M.J.; Williams, M.L.; Lane, E.D. In-situ trace element analysis of monazite and other fine-grained accessory minerals by EPMA. *Chem. Geol.* **2008**, *254*, 197–215. [[CrossRef](#)]
39. Spear, F.S.; Pyle, J.M.; Cherniak, D. Limitations of chemical dating of monazite. *Chem. Geol.* **2009**, *266*, 218–230. [[CrossRef](#)]
40. Schulz, B.; Schüssler, U. Electron-microprobe Th-U-Pb monazite dating in Early-Palaeozoic high-grade gneisses as a completion of U-Pb isotopic ages (Wilson Terrane, Antarctica). *Lithos* **2013**, *175–176*, 178–192. [[CrossRef](#)]
41. Schulz, B.; Krause, J.; Zimmermann, R. Electron microprobe petrochronology of monazite-bearing garnet micaschists in the Oetzal-Stubai Complex (Alpeiner Valley, Stubai). *Swiss J. Geosci.* **2019**, *112*, 597–617. [[CrossRef](#)]

42. Jarosewich, E.; Boatner, L. Rare-Earth Element Reference Samples for Electron Microprobe Analysis. *Geostand. Geoanalytical Res.* **1991**, *15*, 397–399. [[CrossRef](#)]
43. Ludwig, K.R. Users Manual for Isoplot/Ex (rev. 2.49): A Geochronological Toolkit for Microsoft Excel. *Berkeley Geochronol. Cent. Spec. Publ.* **2001**, *1a*, 1–55.
44. Bussy, F.; Hernandez, J.; von Raumer, J. Bimodal magmatism as a consequence of the post-collisional readjustment of the thickened continental lithosphere (Aiguilles Rouges–Mont Blanc Massifs, Western Alps). *Trans. R. Soc. Edinb. Earth Sci.* **2000**, *91*, 221–233.
45. von Raumer, J.; Bussy, F. Mont-Blanc and Aiguilles-Rouges: Geology of their polymetamorphic basement (External massifs, France–Switzerland). *Mém. Géol. (Lausanne)* **2004**, *42*, 1–203.
46. von Raumer, J.; Bussy, F.; Stampfli, G. The Variscan evolution in the External massifs of the Alps and place in their Variscan framework. *Comptes Rendus Geosci.* **2009**, *341*, 239–252. [[CrossRef](#)]
47. Schulz, B.; von Raumer, J.F. Discovery of Ordovician–Silurian metamorphic monazite in garnet metapelites of the Alpine External Aiguilles Rouges Massif. *Swiss J. Geosci.* **2011**, *104*, 67–79. [[CrossRef](#)]
48. Schulz, B. Monazite Microstructures and Their Interpretation in Petrochronology. *Front. Earth Sci.* **2021**, *9*. [[CrossRef](#)]
49. Hoinkes, G.; Thöni, M. Evolution of the Ötztal–Stubai, Scarl–Campo and Ulten Basement Units. In *The Pre-Mesozoic Geology of the Alps*; von Raumer, J.F., Neubauer, F., Eds.; Springer: Berlin/Heidelberg, Germany, 1993; pp. 485–494.
50. Miller, C.; Thöni, M. Origin of eclogites from the Austroalpine Ötztal basement (Tirol, Austria): Geochemistry and Sm–Nd vs. Rb–Sr isotope systematics. *Chem. Geol.* **1995**, *122*, 199–225. [[CrossRef](#)]
51. Neubauer, F. Evolution of late Neoproterozoic to early Palaeozoic tectonic elements in Central and Southeast European Alpine mountain belts: Review and synthesis. *Tectonophysics* **2002**, *352*, 87–103. [[CrossRef](#)]
52. Klötzli-Chowanetz, E.; Klötzli, U.; Koller, F. Lower Ordovician migmatization in the Ötztal crystalline basement (Eastern Alps, Austria): Linking U–Pb and Pb–Pb dating with zircon morphology. *Swiss Bull. Mineral. Petrol* **1997**, *77*, 315–324. [[CrossRef](#)]
53. Thöny, W.F.; Tropper, P.; Schennach, F.; Krenn, E.; Finger, F.; Kaindl, R.; Bernhard, F.; Hoinkes, G. The metamorphic evolution of migmatites from the Ötztal Complex (Tyrol, Austria) and constraints on the timing of the pre-Variscan high-T event in the Eastern Alps. *Swiss J. Geosci.* **2008**, *101*, 111–126. [[CrossRef](#)]
54. Neubauer, F.; Hoinkes, G.; Sassi, F.P. Pre-Alpine metamorphism of the Eastern Alps. *Swiss Bull. Mineral. Petrol* **1999**, *79*, 41–62. [[CrossRef](#)]
55. Tropper, P.; Hoinkes, G. Geothermobarometry of Al₂SiO₅-bearing metapelites in the western Austroalpine Ötztal-basement. *Mineral. Petrol.* **1996**, *58*, 145–170. [[CrossRef](#)]
56. Hoinkes, G.; Koller, F.; Rantitsch, G. Alpine metamorphism of the Eastern Alps. *Swiss Bull. Mineral. Petrol* **1999**, *79*, 155–181. [[CrossRef](#)]
57. Tropper, P.; Recheis, A. Garnet zoning as a window into the metamorphic evolution of a crystalline complex: The northern and central Austroalpine Ötztal-Complex as a polymorphic example. *Mitt. Österr. Geol. Ges.* **2003**, *94*, 27–53.
58. Rode, S.; Rösel, D.; Schulz, B. Constraints on the Variscan P–T evolution by EMP Th–U–Pb monazite dating in the polymetamorphic Austroalpine Ötztal–Stubai basement (Eastern Alps). *German J. Geol.* **2012**, *163*, 43–68. [[CrossRef](#)]
59. Borsi, S.; Del Moro, A.; Sassi, F.P.; Zirpoli, G. Metamorphic evolution of the Austridic rocks to the south of the Tauern Window (Eastern Alps): Radiometric and geopetrologic data. *Mem. Soc. Geol. Ital.* **1973**, *12*, 549–571.
60. Borsi, S.; Del Moro, A.; Sassi, F.P.; Zanferrari, A.; Zirpoli, G. New geopetrologic and radiometric data on the Alpine history of the Austridic continental margin south of the Tauern Window. *Mem. Ist. Geol. Mineral. Univ. Padova* **1978**, *32*, 1–17.
61. Schulz, B. Prograde-retrograde P–T–t-deformation path of Austroalpine micaschists during Variscan continental collision (Eastern Alps). *J. Metamorph. Geol.* **1990**, *8*, 629–643. [[CrossRef](#)]
62. Krenn, E.; Schulz, B.; Finger, F. Three generations of monazite in Austroalpine basement rocks to the south of the Tauern Window: Evidence for Variscan, Permian and Eo-Alpine metamorphic events. *Swiss J. Geosci.* **2012**, *105*, 343–360. [[CrossRef](#)]
63. Schulz, B.; Siegesmund, S.; Steenken, A.; Schönhofer, R.; Heinrichs, T. Geologie des ostalpinen Kristallins südlich des Tauernfensters zwischen Virgental und Pustertal. *Z. Dtsch. Geol. Ges.* **2001**, *152*, 261–307. [[CrossRef](#)]
64. Schulz, B. Mineral chemistry, geothermobarometry and pre-Alpine high-pressure metamorphism of eclogitic amphibolites and mica schists from the Schobergruppe, Austroalpine basement, Eastern Alps. *Miner. Mag.* **1993**, *57*, 189–202. [[CrossRef](#)]
65. Thöni, M. Dating eclogite-facies metamorphism in the Eastern Alps—approaches, results, interpretations: A review. *Miner. Pet.* **2006**, *88*, 123–148. [[CrossRef](#)]
66. Hauke, M.; Froitzheim, N.; Nagel, T.J.; Miladinova, I.; Fassmer, K.; Fonseca, R.O.C.; Sprung, P.; Münker, C. Two high-pressure metamorphic events, Variscan and Alpine, dated by Lu–Hf in an eclogite complex of the Austroalpine nappes (Schobergruppe, Austria). *Acta Diabetol.* **2019**, *108*, 1317–1331. [[CrossRef](#)]
67. Wiesinger, M.; Neubauer, F.; Handler, R. Exhumation of the Saualpe eclogite unit, Eastern Alps: Constraints from 40Ar/39Ar ages and structural investigations. *Miner. Pet.* **2006**, *88*, 149–180. [[CrossRef](#)]
68. Schorn, S.; Stüwe, K. The Plankogel detachment of the Eastern Alps: Petrological evidence for an orogen-scale extension fault. *J. Metamorph. Geol.* **2016**, *34*, 147–166. [[CrossRef](#)]
69. Ratschbacher, L.; Frisch, W.; Neubauer, F.; Schmid, S.M.; Neugebauer, J. Extension in compressional orogenic belts: The eastern Alps. *Geology* **1989**, *17*, 404–407. [[CrossRef](#)]
70. Thoni, M.; Miller, C.H. Garnet Sm–Nd data from the Saualpe and the Koralpe (Eastern Alps, Austria): Chronological and P–T constraints on the thermal and tectonic history. *J. Metamorph. Geol.* **1996**, *14*, 453–466. [[CrossRef](#)]

71. Thöni, M.; Miller, C.; Blichert-Toft, J.; Whitehouse, M.; Konzett, J.; Zanetti, A. Timing of high-pressure metamorphism and exhumation of the eclogite type-locality (Kupplerbrunn–Prickler Halt, Saualpe, south-eastern Austria): Constraints from correlations of the Sm–Nd, Lu–Hf, U–Pb and Rb–Sr isotopic systems. *J. Metamorph. Geol.* **2008**, *26*, 561–581. [[CrossRef](#)]
72. Schuster, R.; Stüwe, K. Permian metamorphic event in the Alps. *Geol.* **2008**, *36*, 603. [[CrossRef](#)]
73. Guan, Q.; Liu, Y.; Neubauer, F.; Li, S.; Genser, J.; Yuan, S.; Chang, R.; Huang, Q.; Fang, Q. Opening of the West Paleo-Tethys Ocean: New insights from earliest Devonian meta-mafic rocks in the Saualpe crystalline basement, Eastern Alps. *Gondwana Res.* **2021**, *97*, 121–137. [[CrossRef](#)]
74. England, P.; Thompson, A.B. Pressure–Temperature–Time Paths of Regional Metamorphism I. Heat Transfer during the Evolution of Regions of Thickened Continental Crust. *J. Pet.* **1984**, *25*, 894–928. [[CrossRef](#)]
75. Thompson, A.B.; England, P. Pressure–Temperature–Time Paths of Regional Metamorphism II. Their Inference and Interpretation using Mineral Assemblages in Metamorphic Rocks. *J. Pet.* **1984**, *25*, 929–955. [[CrossRef](#)]
76. Pyle, J.M.; Spear, F.S.; Rudnick, R.L.; McDonough, W.F. Monazite–Xenotime–Garnet Equilibrium in Metapelites and a New Monazite–Garnet Thermometer. *J. Pet.* **2001**, *42*, 2083–2107. [[CrossRef](#)]
77. Spear, F.S. Monazite–allanite phase relations in metapelites. *Chem. Geol.* **2010**, *279*, 55–62. [[CrossRef](#)]
78. Janots, E.; Brunet, F.; Goffé, B.; Poinssot, C.; Burchard, M.; Cemic, L. Thermochemistry of monazite-(La) and dissakisite-(La): Implications for monazite and allanite stability in metapelites. *Contrib. Miner. Pet.* **2007**, *154*, 1–14. [[CrossRef](#)]
79. Spear, F.S.; Pyle, J.M. Theoretical modeling of monazite growth in a low-Ca metapelite. *Chem. Geol.* **2010**, *273*, 111–119. [[CrossRef](#)]
80. Finger, F.; Krenn, E.; Schulz, B.; Harlov, D.; Schiller, D. “Satellite monazites” in polymetamorphic basement rocks of the Alps: Their origin and petrological significance. *Am. Miner.* **2016**, *101*, 1094–1103. [[CrossRef](#)]
81. Budzyń, B.; Harlov, D.E.; Williams, M.L.; Jercinovic, M.J. Experimental determination of stability relations between monazite, fluorapatite, allanite, and REE-epidote as a function of pressure, temperature, and fluid composition. *Am. Miner.* **2011**, *96*, 1547–1567. [[CrossRef](#)]
82. Knoll, T.; Schuster, R.; Huet, B.; Mali, H.; Onuk, P.; Horschinegg, M.; Ertl, A.; Giester, G. Spodumene Pegmatites and Related Leucogranites from the AustroAlpine Unit (Eastern Alps, Central Europe): Field Relations, Petrography, Geochemistry, and Geochronology. *Can. Miner.* **2018**, *56*, 489–528. [[CrossRef](#)]
83. Chang, R.; Neubauer, F.; Liu, Y.; Genser, J.; Jin, W.; Yuan, S.; Guan, Q.; Huang, Q.; Li, W. Subduction of a rifted passive continental margin: The Pohorje case of Eastern Alps—constraints from geochronology and geochemistry. *Swiss J. Geosci.* **2020**, *113*, 1–25. [[CrossRef](#)]
84. Li, B.; Massonne, H.; Koller, F.; Zhang, J. Metapelite from the high- to ultrahigh-pressure terrane of the Eastern Alps (Pohorje Mountains, Slovenia)—New pressure, temperature and time constraints on a polymetamorphic rock. *J. Metamorph. Geol.* **2021**, *39*, 695–726. [[CrossRef](#)]
85. Ratschbacher, L.; Frisch, W. Palinspastic reconstruction of the pre-Triassic basement units in the Alps: The Eastern Alps. In *Pre-Mesozoic Geology in the Alps*; von Raumer, J.F., Neubauer, F., Eds.; Springer: Berlin/Heidelberg, Germany, 1993; pp. 41–51.